Differential cosmic expansion and the Hubble flow anisotropy

Krzysztof Bolejko,[a] **M. Ahsan Nazer**[b] **and David L. Wiltshire**[b]

[a]Sydney Institute for Astronomy, School of Physics, A28, The University of Sydney, NSW 2006, Australia

[b]Department of Physics and Astronomy, University of Canterbury, Private Bag 4800, Christchurch 8140, New Zealand

E-mail: bolejko@physics.usyd.edu.au, ahsan.nazer@canterbury.ac.nz, david.wiltshire@canterbury.ac.nz

Abstract. The Universe on scales 10–$100\,h^{-1}$Mpc is dominated by a cosmic web of voids, filaments, sheets and knots of galaxy clusters. These structures participate differently in the global expansion of the Universe: from non-expanding clusters to the above average expansion rate of voids. In this paper we characterize Hubble expansion anisotropies in the COMPOSITE sample of 4534 galaxies and clusters. We concentrate on the dipole and quadrupole in the rest frame of the Local Group. These both have statistically significant amplitudes. These anisotropies, and their redshift dependence, cannot be explained solely by a boost of the Local Group in the Friedmann-Lemaître-Robertson-Walker (FLRW) model which expands isotropically in the rest frame of the cosmic microwave background (CMB) radiation. We simulate the local expansion of the Universe with inhomogeneous Szekeres solutions, which match the standard FLRW model on $\gtrsim 100\,h^{-1}$Mpc scales but exhibit nonkinematic relativistic differential expansion on small scales. We restrict models to be consistent with observed CMB temperature anisotropies, while simultaneously fitting the redshift variation of the Hubble expansion dipole. We include features to account for both the Local Void and the "Great Attractor". While this naturally accounts for the Hubble expansion and CMB dipoles, the simulated quadrupoles are smaller than observed. Further refinement to incorporate additional structures may improve this. This would enable a test of the hypothesis that some large angle CMB anomalies result from failing to treat the relativistic differential expansion of the background geometry; a natural feature of solutions to Einstein's equations not included in the current standard model of cosmology.

Contents

1 Introduction

In cosmology deviations from a uniform expansion are most commonly treated as peculiar velocities relative to a linear Hubble law

$$v_{\rm pec} = cz - H_0 r \tag{1.1}$$

where z is the redshift, c the speed of light, r an appropriate distance measure, and $H_0 \equiv H(t_0) = 100\, h\, {\rm km\, s^{-1}\, Mpc^{-1}}$ is the Hubble constant, h being a dimensionless number. Such a theoretical framework is a natural description if the assumption of homogeneity and isotropy holds at all scales, so that all cosmologically relevant motions can be understood in terms the background expansion of one single Friedmann–Lemaître–Robertson–Walker (FLRW) geometry, with a Hubble parameter, $H(t)$, given by the Friedmann equation, plus local boosts which can be treated by eq. (1.1) for suitably small values of the distance,[1] r.

However, on scales of tens of megaparsecs the Universe exhibits strong inhomogeneities, dominated in volume by voids with density contrasts close to the minimum possible $\delta\rho/\rho =$

---

[1]Even within FLRW models, for large values of r one has to take into account that $H(t)$ varies with time, and that the redshift is not additive but rather a multiplicative quantity, so a simple addition as in (1.1) does not apply: $1 + z_{1+2} = (1 + z_1)(1 + z_2) \neq 1 + z_1 + z_2$.

−1 [1–4]. Galaxies and galaxy clusters are not randomly distributed but are strung in filaments that thread and surround the voids to form a complex cosmic web [5–7]. The Universe is only spatially homogeneous is some statistical sense when one averages on scales $\gtrsim 100\,h^{-1}$Mpc. Just how large this scale is, is debated [8–12]. However, based on the fractal dimension of the 2–point galaxy correlation function making a gradual transition to the homogeneous limit $D_2 \to 3$ in three spatial dimensions, a scale of statistical homogeneity in the range $70 \lesssim r_{\rm ssh} \lesssim 120\,h^{-1}$Mpc seems to be observed [10].

Despite the fact that the FLRW geometry can only be observationally justified on $\gtrsim 100\,h^{-1}$Mpc scales, by tradition it is conventionally assumed that such a geometry is still applicable at all scales on which space is expanding below $r_{\rm ssh} \sim 100\,h^{-1}$Mpc, that is, until one gets to the very small scales of bound clusters of galaxies. However, this assumption is not justified by the principles of general relativity. In general, in solutions of Einstein's equations the background space does not expand rigidly to maintain constant spatial curvature as it does in the FLRW geometry. General inhomogeneous cosmological models, such as the Lemaître–Tolman (LT) [13–15] and Szekeres [16] models, exhibit differential cosmic expansion. The Hubble parameter becomes a function of space as well as time, and any relation (1.1) can no longer have the physical sense of defining a peculiar velocity field with respect to a single expansion rate.

In this paper we will present the results of numerical investigations that quantify the nonlinearity associated with differential cosmic expansion in Szekeres solutions chosen to match key features of both the Cosmic Microwave Background (CMB) anisotropies, and also the Hubble expansion on $\lesssim 100\,h^{-1}$Mpc scales. The crucial feature in these simulations is that the dipole induced by local inhomogeneities cannot be directly attributed to a $635\,{\rm km\,s^{-1}}$ local boost of the Local Group (LG) of galaxies, and is thus nonkinematic (as we define more precisely in Section 2.1 below).

Despite its naturalness in general relativity, the hypothesis of a nonkinematic origin for a fraction of the CMB dipole goes against the consensus of what has been assumed in observational cosmology [17, 18] ever since the first bounds were placed on the anisotropy of the CMB in the 1960s [19]. By now it is standard practice to automatically transform redshift data to the CMB rest frame before performing cosmological analyses.

Within the standard peculiar velocities framework, the amplitude of bulk flows, their consistency with the standard Lambda Cold Dark Matter (ΛCDM) cosmology and their convergence to the CMB frame, are matters of ongoing debate [20–31]. A possible nonkinematic origin for a fraction of the CMB dipole would impact directly on this debate, as well as suggesting a reexamination of other observational puzzles. Arguably the most important of these are the large angle anomalies that have been observed in the CMB anisotropy spectrum for over a decade [32–41], with a statistical significance that has increased with the release of Planck satellite data [42–44].

The hypothesis that a fraction of the local Hubble expansion is nonkinematic should be subject to appropriate observational tests. In recent work [45, 46] we devised such tests and found very strong Bayesian evidence for the nonkinematic hypothesis. In an independent study [47], the hypothesis of a purely kinematic origin for the dipole in the cosmic distribution of radio galaxies has been rejected at the 99.5% confidence level.

In order to develop more powerful tests of the nonkinematic differential expansion hypothesis, in this paper we will use exact solutions of Einstein's equations for structures smaller than the statistical homogeneity scale [10] for the purpose of ray–tracing simulations.

There have been a number of previous studies which have used the LT solution to model

the effects of anisotropic expansion [48–55], including its effects on the CMB. However, these have typically considered the effects of voids at large distances from our location, or the effects of voids much larger than the small scale inhomogeneities we will consider.

To our knowledge this paper contains the first ever study which seeks to use exact solutions of Einstein's equations to model structures giving rise to nonlinear expansion on scales comparable to those observed, constrained directly by both ray–tracing of the CMB and by the Hubble expansion field from actual surveys. While the Szekeres solution has been employed for a number of cosmological problems [56–65], we believe that this is also the first time that it has been used for ray–tracing simulations of local structures. We will see that although we are not able to match all features of the nonlinear Hubble expansion below the statistical homogeneity scale, with the Szekeres solution we can nonetheless match more features of the actual data than with other models, including the standard FLRW cosmology with a local boost of the Local Group of galaxies.

This paper provides a proof–of–principle demonstration that we hope will encourage even more sophisticated investigations of relativistic effects beyond the perturbed FLRW model. Some potential future investigations are outlined in Sec. 5.

2 Terminology

In this paper we often use terms such as *nonlinear* and *nonkinematic*. These terms are ambiguous and therefore this Section describes how these terms are defined in this paper.

2.1 Nonkinematic and relativistic differential expansion

The fact that cosmic expansion can vary not only in time but in space leads to a variation in the redshift of observed astronomical sources, be they galaxies or the CMB. If the redshift of an observed object can be described solely in terms of a homogeneous expansion and a Doppler effect, then we would call the redshift anisotropy *kinematic*:

$$(1+z)_{\text{obs}} = (1+z)_{\text{FLRW}}(1+z)_{\text{Doppler}} . \tag{2.1}$$

The first redshift term on the right hand side refers to the global homogeneous and isotropic expansion of the FLRW model, and second term is due to a Doppler effect with respect to the FLRW background that combines the motions of the observer (local boost) and the observed object (peculiar motion). If the redshift of an observed source (galaxies or CMB) cannot be explained entirely in terms of the above equation then *nonkinematic* effects are present, be they a real physical phenomenon or merely some observational bias[2].

The factor $(1+z)_{\text{FLRW}}$ in (2.1) can only be defined with respect to a canonical choice of our local Lorentz frame. Since the CMB is remarkably isotropic, with a dipole of amplitude $1.23 \times 10^{-3} T_0$ of the mean temperature $T_0 = 2.725\,\text{K}$, the canonical *CMB rest frame* is defined by matching the $3.37\,\text{mK}$ temperature dipole to the dipole in the series expansion

$$\frac{T_0}{\gamma_{\text{CMB}}(1 - \beta_{\text{CMB}} \cos\theta)} = T_0 \left[1 + \beta_{\text{CMB}} \cos\theta + \beta_{\text{CMB}}^2 \left(\cos^2\theta - \frac{1}{2}\right) + \ldots\right] \tag{2.2}$$

---

[2]We assume all observational biases can be accounted for, although this requires care in actual data analysis [46]. We deal only with the case of real physical effects in this paper. Furthermore, while all galaxies within larger bound clusters will still be assumed to exhibit peculiar local motions within each cluster, for nonkinematic redshift anisotropies we are only interested in redshifts and distances assigned collectively to gravitationally bound structures.

where $\beta_{\mathrm{CMB}}\cos\theta \equiv \boldsymbol{\beta}_{\mathrm{CMB}}\cdot\hat{\boldsymbol{n}}_{\mathrm{hel}}$, $\hat{\boldsymbol{n}}_{\mathrm{hel}}$ is the unit vector on the sky in the heliocentric frame, $\boldsymbol{\beta}_{\mathrm{CMB}} = \boldsymbol{v}_{\mathrm{CMB}}/c$ is the boost vector of the CMB frame in the heliocentric frame, and $\gamma_{\mathrm{CMB}} = (1 - \beta_{\mathrm{CMB}}^2)^{-1/2}$ is the standard Lorentz gamma factor.

Using measurements of redshifts and distances of galaxy clusters, one can independently define the local *average isotropic expansion (AIE) frame* as the Lorentz frame at our location in which the spherically averaged distance–redshift relation in independent radial shells has minimal variations relative to a linear Hubble law [45, 46]. Since isotropy is only defined by an average then the observed redshift of any individual source will in general display a nonkinematic anisotropy differing from (2.1) with a dependence, $z(\hat{\boldsymbol{n}}_{\mathrm{AIE}})$, on the unit vector on the sky in the AIE frame, $\hat{\boldsymbol{n}}_{\mathrm{AIE}}$.

According to (2.1), even a perturbed FLRW model will display nonkinematic effects. However, such effects are small and are not expected to affect the identification of the dipole in (2.2). In this paper, we will study models with nonkinematic effects that we will characterize in terms of the variation of averages of the nearby Hubble expansion. These nonkinematic effects will turn out to be so large that they are also likely to be distinguishable when compared to perturbed FLRW models, offering a simple alternative characterization. In particular, if we make a boost from the AIE frame to the heliocentric frame of our own measurements then the difference of the CMB temperature dipole and the standard kinematic dipole identified by (2.2) can be observationally significant.

We will therefore define *general relativistic nonkinematic differential expansion* (or more succinctly *relativistic differential expansion*) to occur when the difference

$$\Delta T_{\mathrm{nk-hel}} = \frac{T_{\mathrm{AIE}}}{\gamma_{\mathrm{AIE}}(1 - \boldsymbol{\beta}_{\mathrm{AIE}}\cdot\hat{\boldsymbol{n}}_{\mathrm{hel}})} - \frac{T_0}{\gamma_{\mathrm{CMB}}(1 - \boldsymbol{\beta}_{\mathrm{CMB}}\cdot\hat{\boldsymbol{n}}_{\mathrm{hel}})} \tag{2.3}$$

has a measurably nonzero dipole when expanded in spherical harmonics[3], where $\boldsymbol{\beta}_{\mathrm{AIE}} = \boldsymbol{v}_{\mathrm{AIE}}/c$ is the boost of the AIE frame in the heliocentric frame, $\gamma_{\mathrm{AIE}} = (1 - \beta_{\mathrm{AIE}}^2)^{-1/2}$, and

$$T_{\mathrm{AIE}}(\hat{\boldsymbol{n}}_{\mathrm{AIE}}) = \frac{T_{\mathrm{CMB}}}{1 + z_{\mathrm{AIE}}(\hat{\boldsymbol{n}}_{\mathrm{AIE}})}\,, \tag{2.4}$$

is the anisotropic CMB temperature as measured in the AIE frame. Here $T_{\mathrm{CMB}} = (1+z_{\mathrm{dec}})T_0$ is the mean intrinsic temperature of the primordial plasma at decoupling, z_{dec} being the constant isotropic redshift of decoupling in the FLRW model. In practice, "measurably nonzero" here means a contribution to (2.3) of at the least the same level, $10^{-5}T_0$, as the primordial spectrum; i.e., one order of magnitude larger than the boost dipole in (2.2).

This an operational model–independent[4] definition. Since eq. (2.4) does not separate out the primordial CMB anisotropies, our definition cannot distinguish a primordial CMB dipole from "local" nonkinematic relativistic effects. However, we will construct numerical solutions constrained by large galaxy surveys, leading to direct predictions for the amplitude and direction of the nonkinematic dipole in terms of general relativity alone, rather than by appealing to unknown physics in the early Universe.

---

[3]By construction (2.3) has zero monopole.

[4]The definition applies not only to exact solutions of Einstein's equations, but to any cosmological model with a close to linear Hubble law, including models with backreaction such as the timescape model [67–70]. One could further refine this definition to treat the quadrupole and small frequency dependent effects of a boost on the black body spectrum [71]. However, as yet we are unable to distinguish such terms given current knowledge of the modelling of foregrounds such as galactic dust.

Once one accounts for the known motions of the Sun and Milky Way within the bound system that forms the Local Group of galaxies, to explain the observed dipole in (2.2) the LG has to move with a velocity

$$v_{\mathrm{o}} = 635 \pm 38 \, \mathrm{km\,s^{-1}} \tag{2.5}$$

in the direction

$$(\ell_{\mathrm{o}}, b_{\mathrm{o}}) = (276.4^{\circ}, 29.3^{\circ}) \pm 3.2^{\circ}, \tag{2.6}$$

in galactic coordinates [66]. The results of [45, 46] show that the CMB and AIE frames are statistically significantly different, while the LG frame cannot be statistically distinguished from the AIE frame given uncertainties in the data. Thus if we take the LG frame as the AIE frame then (2.3) will involve the subtraction of two milli-Kelvin anisotropies, one of which is nonkinematic, leaving a residual which is likely to be observationally significant.

Our numerical simulations are not yet sophisticated enough that we will apply (2.3) directly to sky maps. For the purpose of our numerical simulations we will assume that the average isotropic expansion frame coincides with the LG frame, so that $T_{\mathrm{LG}} = T_{\mathrm{AIE}}$ and $\hat{\boldsymbol{n}}_{\mathrm{LG}} = \hat{\boldsymbol{n}}_{\mathrm{AIE}}$ as given by (2.4). Furthermore, rather than working in the heliocentric frame, we will work in the LG frame and constrain the CMB dipole and quadrupole of (2.4) directly by ray tracing.

2.2 Large scale homogeneous isotropic distance–redshift nonlinearity

Independently of the energy momentum tensor, the luminosity distance relation of any FLRW cosmology can be Taylor expanded at low redshifts to give

$$d_L(z) = \frac{c}{H_0} \left\{ z + \frac{1}{2} \left[1 - q_0 \right] z^2 - \frac{1}{6} \left[1 - q_0 - 3q_0{}^2 + j_0 + \frac{kc^2}{H_0{}^2 a_0{}^2} \right] z^3 + O(z^4) \right\} \tag{2.7}$$

where d_L is the luminosity distance to the observed galaxy, q_0 the deceleration parameter, j_0 the jerk parameter, $a_0 = a(t_0)$ the present cosmic scale factor, and $k = -1, 0, 1$ the spatial curvature. The $O(z^2)$ and higher order terms represent nonlinear corrections to the linear Hubble law.

Even if the Universe is not described by a FLRW model, but by some alternative in which a notion of statistical homogeneity applies, then we can still expect a cosmic expansion law with a Taylor series in z similar to (2.7). This is the case for the timescape cosmology [67–70], for example. However, in such cases the higher order coefficients will not have the form given in (2.7). In particular, generically averages of inhomogeneous models do not expand in such a way as to maintain a rigid constant spatial curvature, k.

2.3 Small scale nonlinearities: the "nonlinear regime"

Even if the FLRW model is a good fit on large scales, the Taylor expansion (2.7) is only *a priori* justified on scales $d_L \gtrsim r_{\mathrm{ssh}}$ on which a notion of statistical homogeneity applies. Small scale differences will lead to complex deviations from an average linear Hubble expansion. In the perturbed FLRW model such deviations are induced on small scales when density perturbations become nonlinear, giving rise to the *nonlinear regime* of perturbation theory.

In the standard cosmology small scale nonlinear cosmic expansion is investigated with large N-body numerical simulations using Newtonian gravity in a uniformly expanding box, with an expansion rate fit to a FLRW model. While any form of nonlinear expansion might be

interpreted as "differential expansion", by construction the N–body simulations can always be interpreted in terms of small scale flows in which velocities are added with respect to the assumed FLRW background. Such models do not allow the possibility of a relativistic differential expansion as defined by eqs. (2.3), (2.4). The characterization of the differences between N-body simulations and the models of this paper will be left to future work [72].

In the present paper, we are interested in the observational scales which are usually interpreted in the nonlinear regime of perturbed FLRW models, but we make different model assumptions to interpret the observations. Regardless of the assumed cosmological model, we use the term *nonlinear regime* to apply to redshift–space distortions due to nonlinear expansion on scales of tens of megaparsecs that affect all cosmological observations. For more distant objects the redshift–space distortions at the source will lead to small uncertainties as a fraction of the overall distance. However, in our own vicinity on scales $d_L \lesssim r_{\rm ssh}$ these effects can be large.

In order to construct any numerical simulation some model is required. In this paper, we will perform simulations with the Szekeres solution, which does allow for a relativistic nonkinematic differential expansion. However, we will first discuss the recent model–independent investigation of the Hubble expansion in the nonlinear regime, which motivated the present study.

2.4 Model independent characterization of small scale nonlinear expansion

In recent work [45, 46] the problem of characterizing the Hubble expansion below $r_{\rm ssh}$ was approached with no prior assumptions about the homogeneity of the spatial geometry. In particular, given a large data set with good sky coverage, one can simply determine the best fit average linear Hubble law in radial shells, even in the regime in which the expansion is nonlinear, a technique first used by Li and Schwarz [73]. Another alternative is to take angular averages, for example, by employing a Gaussian window averaging method pioneered by McClure and Dyer [74].

Wiltshire et al. [45] applied these techniques to the COMPOSITE sample of 4,534 galaxies and clusters compiled from earlier surveys by Watkins et al. [20, 75]. A startling result was found — when the best fit spherically averaged Hubble parameter in inner shells was compared to the asymptotic value on $r > 156\,h^{-1}$Mpc scales, it was found that the Hubble expansion was more uniform in the rest frame of the Local Group (LG) of galaxies than in the standard CMB rest frame, with very strong Bayesian evidence. There is no reason why this should be true in the standard cosmology. It is expected that the CMB rest frame should coincide with the local frame in which the Hubble expansion is most uniform, with minimum statistical variations.

It was argued by Wiltshire et al. [45] that an arbitrary boost, v, of the central observer from a rest frame in which the Hubble parameter, H, is close to uniform will display a systematic offset of the value H' determined by least squares regression in spherical shells in the boosted frame. In particular, when minimizing the sum $\chi_s^2 = \sum_i \left[\sigma_i^{-1}(r_i - cz_i'/H')\right]^2$ with respect to H', where r_i and σ_i are individual distances and their uncertainties, under a boost of the central observer the original redshifts transform as $cz_i \to cz_i' = cz_i + v\cos\phi_i$ for small v, where ϕ_i is the angle between each data point and the boost direction. Provided the number density of objects in a distance catalogue is balanced on opposite sides of the sky, then terms linear in the boost cancel from opposite sides of the sky in a spherical average,

leaving a term proportional to v^2. The offset is found to give approximately

$$H' - H \simeq \frac{v^2}{2\bar{H}_0 \langle r_i^2 \rangle},$$
(2.8)

in successive radial shells, where $\bar{H}_0$ is the asymptotic Hubble constant in the range where expansion is linear. McKay and Wiltshire [46] found that such a signature is indeed observed between the CMB and LG rest frames in both the COMPOSITE sample [20, 75], and in the larger *Cosmicflows-II* (CF2) sample [76].

It was also found by Wiltshire et al. [45] that the largest residual monopole variation in the Hubble expansion in the LG rest frame occurs in a range $40\,h^{-1}$ – $60\,h^{-1}$Mpc, whereas the monopole variation in the CMB frame is less than in the LG frame in this range only. Over the same distance range $H' - H$ is found to deviate from the relation (2.8) in both the COMPOSITE and CF2 catalogues[5]. Angular averages reveal a dipole structure in the Hubble expansion, whose amplitude changes markedly over the range $32\,h^{-1}$ – $62\,h^{-1}$Mpc, in different ways in the two rest frames. The conclusion from various analyses [45] is that the boost from the LG frame to the CMB frame appears to be compensating for the effect on cosmic expansion of inhomogeneous structures within this distance range. A boost to the CMB frame has the effect of almost cancelling the monopole and dipole variations; but not perfectly. Whereas the amplitude of the dipole expansion variation declines to levels statistically consistent with zero for $r \gtrsim 65\,h^{-1}$Mpc in the LG frame, in the CMB frame the dipole amplitude drops to a minimum value close to zero at $r \sim 44\,h^{-1}$Mpc, but subsequently increases [45].

Finally, using Gaussian window averages, a sky map of angular Hubble expansion variation on $r > 15\,h^{-1}$Mpc scales was determined for the COMPOSITE sample and its correlation coefficient, $\mathcal{C}$, with the residual CMB dipole in the LG frame was computed. It was found that $\mathcal{C} = -0.92$ for an angular smoothing scale $\sigma_\theta = 25°$, which was almost unchanged as the smoothing scale was varied in the range $15° < \sigma_\theta < 40°$.

The combination of the above results led to the hypothesis of Wiltshire et al. [45] that a significant component of the observed CMB dipole, which is conventionally attributed to a local boost (2.5), (2.6) of the Local Group of galaxies, is nonkinematic in origin. It should be attributed to a differential expansion of space, due to foreground inhomogeneities on $\lesssim 65\,h^{-1}$Mpc scales which result in a 0.5% anisotropy in the distance–redshift relation below these scales.

From the point of view of general relativity, such a hypothesis is not surprising — it is simply a property of general inhomogeneous cosmological models. Indeed, using a simple Newtonian approximation [52] for LT models [13–15], numerical estimates of the size of the effect were made by Wiltshire et al. [45]. These were indeed consistent observationally both in terms of the magnitude of the CMB temperature dipole and quadrupole, and the scale of the void relative to that of the actual structures observed in the nearby Universe [77].

---

[5]The reported CF2 distances include untreated distribution Malmquist biases [76] which lead to an additional spurious monopole [30, 46] when spherical averages are taken. Despite this bias the signature (2.8) is still apparent in the CF2 catalogue in the *difference* $H' - H$, but with a somewhat broader distance range, $30\,h^{-1} \lesssim r \lesssim 67\,h^{-1}$Mpc, over which (2.8) does not apply, consistent with there being additional systematic uncertainties in individual distances [46].

3 The observational data

3.1 The anisotropy of the Hubble expansion

At low redshifts the Hubble constant for a spatially flat FLRW universe can be calculated by rearranging the terms of (2.7) to obtain

$$H_0 = \frac{c}{d_L}\left[z + \frac{1}{2}(1-q_0)z^2 - \frac{1}{6}(1-q_0-3q_0^2+j_0)z^3\right]. \tag{3.1}$$

Given a large set of data with independently measured values of z and d_L one could determine H_0, q_0 and j_0 for any spatially homogeneous isotropic cosmology using the above formula. In practice, with current data one is only able to independently determine H_0 at low redshifts, and when terms beyond the linear Hubble law are used in (3.1) then fixed values of q_0 and j_0 must be assumed from other observations. For example, the SH0ES [78] estimate assumes values $q_0 = -0.55$ and $j_0 = 1$ consistent with a spatially flat FLRW model with $\Omega_m = 0.3$. In the present paper, we use $q_0 = -0.5275$ and $j_0 = 1$, consistent with the best fit value $\Omega_m = 0.315$ of Ade et al. [79].

As seen from Fig. 1, except for the Zone of Avoidance region obscured by our Galaxy ($|b| \lesssim 15°$), the COMPOSITE sample has good angular coverage[6], and thus can be used to evaluate large angle anisotropies of the Hubble expansion (dipole and quadrupole). However, the COMPOSITE sample has large uncertainties associated with the distance measure.

From the point of view of propagation of uncertainty, it is better to work with the formula (2.7) with d_L as the independent variable in the numerator. To infer H_0 from the data we therefore minimize the following sum

$$\chi^2 = \sum_i \left(\frac{d_i - c\zeta_i/H_0}{\Delta d_i}\right)^2, \tag{3.2}$$

where

$$\zeta_i = \left[z_i + \frac{1}{2}(1-q_0)z_i^2 - \frac{1}{6}(1-q_0-3q_0^2+j_0)z_i^3\right], \tag{3.3}$$

d_i and z_i are respectively the luminosity distance and redshift of each object in the COMPOSITE sample, and Δd_i is the distance uncertainty. The above is equivalent to calculating the Hubble constant as a weighted average,

$$H_0 = \frac{\sum_i H_i w_{d,i}}{\sum_i w_{d,i}}, \tag{3.4}$$

where

$$H_i = c\zeta_i/d_i \tag{3.5}$$

and

$$w_{d,i} = c\zeta_i d_i/(\Delta d_i)^2. \tag{3.6}$$

Wiltshire et al. [45] evaluated (3.4) for spherical averages in independent radial shells, for the case of a linear Hubble law with $\zeta_i = z_i$, and separately considered angular averages using a Gaussian window function smoothing in solid angle.

---

[6]This statement remains true when the data is broken into concentric radial shells in distance, as is seen in Fig. 2 of Wiltshire et al. [45], where only the innermost of 11 radial shells (with $d_L < 18.75\,h^{-1}\text{Mpc}$) was found to have insufficient sky coverage when performing statistical checks.
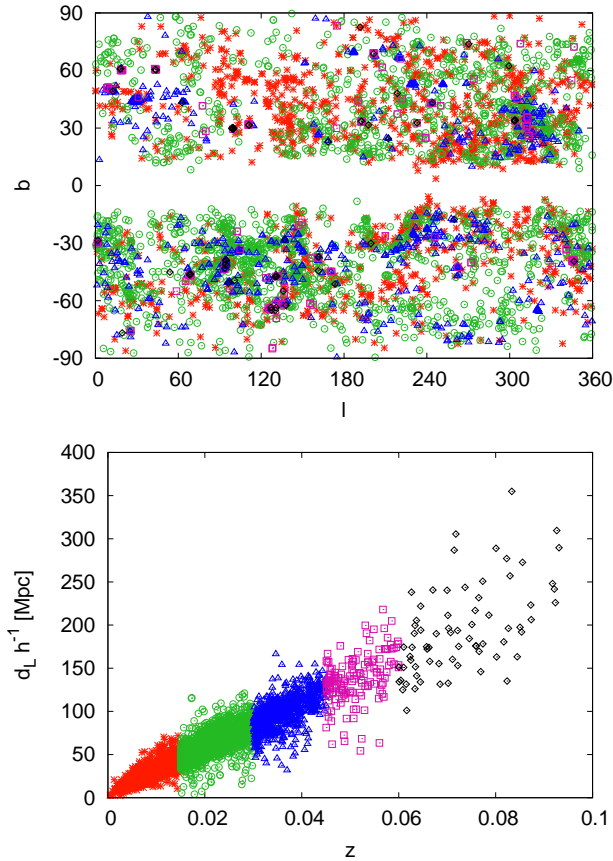
Figure 1. The COMPOSITE sample. *Upper Panel*: angular distribution of galaxies in the Galactic coordinates ℓ and b; *Lower Panel*: distance vs LG frame redshift; $z \leq 0.015$ red stars, $0.015 < z \leq 0.03$ green circles, $0.03 < z \leq 0.045$ blue triangle, $0.045 < z \leq 0.06$ magenta square, $z > 0.06$ black diamonds.

Here we will apply Gaussian window function smoothing jointly in both solid angle and redshift, to obtain the following formula for the average local Hubble constant centred at galactic coordinates (ℓ, b) and redshift, z,

$$H_0(\ell, b, z) = \frac{\sum_i H_i w_{d,i} w_{z,i} w_{\theta,i}}{\sum_i w_{d,i} w_{z,i} w_{\theta,i}}, \tag{3.7}$$

where H_i and $w_{d,i}$ are given by (3.5) and (3.6) respectively, while

$$w_{z,i} = \frac{1}{\sqrt{2\pi}\sigma_z} \exp\left[-\frac{1}{2}\left(\frac{z - z_i}{\sigma_z}\right)^2\right], \tag{3.8}$$

$$w_{\theta,i} = \frac{1}{\sqrt{2\pi}\sigma_\theta} \exp\left[-\frac{1}{2}\left(\frac{\theta_i}{\sigma_\theta}\right)^2\right], \tag{3.9}$$

$\sigma_z = 0.01$, $\sigma_\theta = 25°$, and θ_i is the angle between the direction of each source (ℓ_i, b_i) and the direction of any given point on the sky, (ℓ, b):

$$\cos\theta_i = \cos b \cos b_i \cos(\ell - \ell_i) + \sin b \sin b_i.$$

For $w_{z,i} = 1$ — i.e., with no redshift smoothing — equations (3.7) and (3.9) reduce to equations (B5) and (B9) derived in Appendix B of ref. [45] using a procedure based on minimizing the scatter in H^{-1}.

Using (3.7) we calculate the regional contributions to our locally measured Hubble constant on an angular and redshift grid. For each redshift value on the grid, we construct the angular maps of the Hubble expansion and express the Hubble flow in terms of its fluctuations

$$\frac{\Delta H_0}{\langle H_0 \rangle} = \frac{H_0(\ell, b, z) - \langle H_0 \rangle}{\langle H_0 \rangle},\tag{3.10}$$

where

$$\langle H_0 \rangle = \frac{\int \mathrm{d}\Omega \, H_0(\ell, b, z)}{4\pi},\tag{3.11}$$

is the spherically averaged value of (3.7).

For each redshift, the fluctuations (3.10) are then analysed using the spherical harmonic decomposition

$$\frac{\Delta H_0}{H_0} = \sum_{l,m} a_{lm} Y_{lm},\tag{3.12}$$

which allows us to evaluate the angular power spectrum:

$$C_l = \frac{1}{2l+1} \sum_m |a_{lm}|^2.\tag{3.13}$$

The power spectrum obtained in this way is subject to several biases and uncertainties [80]

$$C_l = \sum_{l'} M_{ll'} B_{l'}^2 \mathcal{C}_{l'} + N_{l'}\tag{3.14}$$

where $\mathcal{C}_{l'}$ is the true underlying power spectrum, $M_{ll'}$ describes the mode–mode coupling resulting from incomplete sky coverage, B_l is a window function due to the smoothing, and N_l is the noise. As seen in Fig. 1 for $|b| \lesssim 15°$ data is incomplete in the galactic plane. In this paper, we do not mask these regions. Instead we extrapolate data to these regions using Gaussian smoothing of radius $\sigma_\theta = 25°$, as follows from eq. (3.14). While this can potentially affect the inferred power spectrum, for the large angular scales (such as dipole and quadrupole) of interest here the results are not significantly altered [45]. As for the noise, we estimate the level of contamination of the power spectrum due to distance uncertainties and number of data in the next section.

3.2 Completeness and robustness

As seen from Fig. 1, and in more detail in Fig. 2 of Wiltshire et al. [45], there is good angular coverage in the COMPOSITE data. Potential systematic uncertainties from anisotropies generated by insufficient sky cover were investigated in detail by Wiltshire et al. [45], who performed 12 million random reshuffles of the data in independent spherical shells, with the conclusion that for a binning scale $\Delta d = 12.5 \, h^{-1}\mathrm{Mpc}$ (or $\Delta z \simeq 0.004$) results concerning the dipole anisotropy were robust on scales $0.002 < z < 0.04$, with up to 99.999% confidence in some ranges.

In our case, we are also investigating the quadrupole anisotropy and adopt the larger redshift smoothing scale $\Delta z = 0.01$. However, there is still a possibility that the inferred

anisotropy could result from some biases in the data. To minimize any systematic bias and to confirm that the measured anisotropy is not spurious, we performed the following checks:

- We used the fluctuations (3.12) rather than the spherical average (3.4). In the hypothetical case of an exactly homogeneous and isotropic universe (and perfect measurements) $\Delta H_0 = 0$, so even if we have all the data only in one part of the sky and the rest of the sky without any measurement we should not detect any anisotropy.

- We shuffled the data. We tested the robustness of the results on the dipole and quadrupole anisotropies by analyzing the reshuffled data — for each pair of z and d_L we randomly reshuffled the angular position. We generated 100,000 reshuffled COMPOSITE catalogues and calculated the dipole and quadrupole of the Hubble expansion. If the measured signal were comparable with the signal obtained from reshuffled samples that would indicate that the original result is spurious. That was not the case, however.

- We used half of the data. An alternative test of robustness was performed by taking half of the COMPOSITE sample to calculate the dipole and quadrupole anisotropies of the Hubble expansion. This was done for 100,000 randomly selected halves of the original COMPOSITE catalogue. If the measured signal was not consistent with the anisotropy obtained from half of the sample that would indicate that the original result is spurious. Again, this was not the case.

The results of the above analyses are combined in Fig. 2. As seen our analysis passes these tests at the 2σ level for $z \lesssim 0.045$. This is consistent with the more exhaustive tests of Wiltshire et al. [45], which showed that the dipole is not a systematic effect, to very high confidence.

3.3 Kinematic interpretation of anisotropies

The results presented in Fig. 2 indicate the presence of anisotropy in the Hubble expansion up to $z \sim 0.045$, as determined from the COMPOSITE sample redshifts transformed to the LG rest frame. The anisotropy is largest for small redshifts $z \sim 0.02$, with the amplitude of the dipole dropping one order of magnitude from $z = 0.02$ to $z = 0.045$, from which point the dipole amplitude is consistent with that of the randomly reshuffled data at 2σ.

According to the conventional explanation the anisotropy of the Hubble expansion observed in Fig. 2 should have a kinematic origin, due to a boost (2.5), (2.6) from the LG to CMB rest frame. This hypothesis can be directly tested by assuming a spatially homogeneous universe in the CMB frame, generating mock COMPOSITE samples in that frame, adjusting the redshift by performing a local boost to the LG frame, and then analysing the mock data in the manner of Fig. 2. Specifically,

1. We take the COMPOSITE sample. For each galaxy we have its angular position (ℓ_i, b_i), luminosity distance d_i, uncertainty in distance Δd_i and redshift z_i. For each of these directions (ℓ_i, b_i) we use the FLRW model to find the redshift (z_{FLRW}) at which $d_L = d_i$, by solving

$$d_L = (1+z)\frac{c}{H_0} \int\limits_0^{z_{\text{FLRW}}} dz \frac{1}{\sqrt{\Omega_m(1+z)^3 + 1 - \Omega_m}},$$
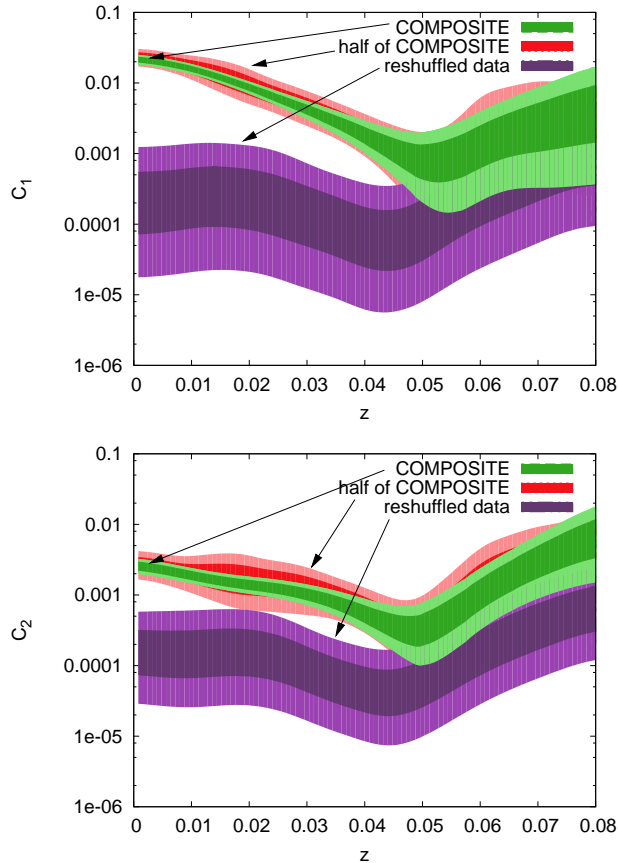
Figure 2. The anisotropy of the Hubble expansion in the LG frame: dipole (*Upper Panel*) and quadrupole (*Lower Panel*). The green bands show the 65% and 95% confidence intervals for the COMPOSITE sample. The red bands show the 65% and 95% confidence intervals obtained using 100,000 random halves of the COMPOSITE sample. The purple bands show the 65% and 95% confidence intervals obtained using 100,000 random reshuffles of the COMPOSITE sample.

with $\Omega_m = 0.315$, corresponding to the best fit parameters from the Planck satellite [79]. (We also take the Planck satellite normalized $H_0 = 67.3 \, \mathrm{km \, s^{-1} \, Mpc^{-1}}$. However, since we normalize all distances to $h^{-1}\mathrm{Mpc}$, this is inconsequential.)
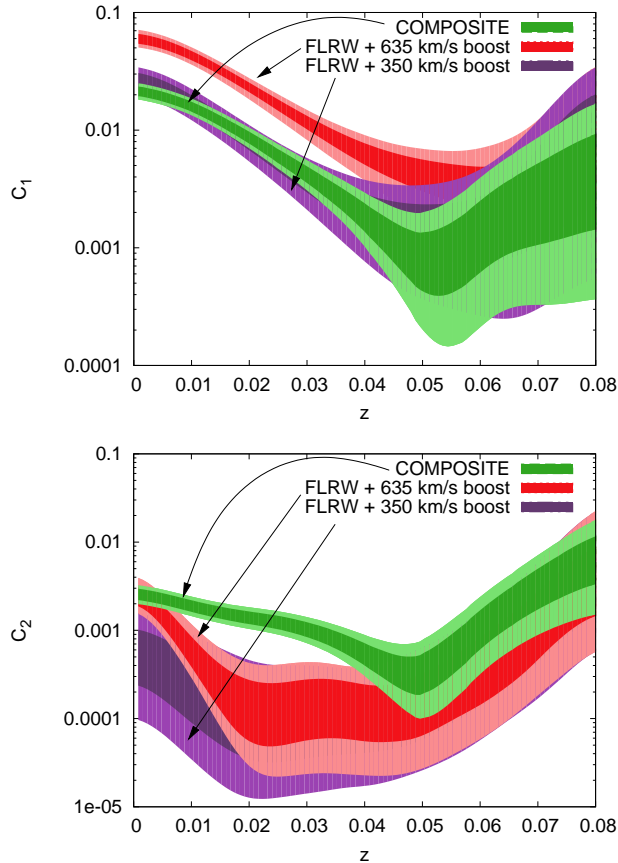
2. We adjust the redshift for the local boost

$$
\begin{aligned}
1 + z_{\mathrm{FLRW-B}} &= \gamma(1 - \beta_{\mathrm{o}} \cos\theta)(1 + z_{\mathrm{FLRW}}) \\
&\simeq (1 - \beta_{\mathrm{o}} \cos\theta)(1 + z_{\mathrm{FLRW}}),
\end{aligned}
\tag{3.15}
$$

where $\beta_{\mathrm{o}} = v_{\mathrm{o}}/c = (2.1 \pm 0.1) \times 10^{-3}$ by (2.5), while

$$
\cos\theta = \cos b_{\mathrm{o}} \cos b_i \cos(\ell_{\mathrm{o}} - \ell_i) + \sin b_{\mathrm{o}} \sin b_i,
$$

ℓ_{o} and b_{o} being given by (2.6), and we have set $\gamma = \left(1 - \beta_{\mathrm{o}}^2\right)^{-1/2} \simeq 1$, ignoring terms of $\mathrm{O}(\beta_{\mathrm{o}}^2)$.

3. We construct a mock COMPOSITE catalogue in the LG frame, by replacing z_i with $z_{\mathrm{FLRW-B}}$, (i.e., the redshift obtained in the FLRW model adjusted for the LG motion).

Figure 3. The anisotropy of the Hubble expansion: dipole (*Upper Panel*) and quadrupole (*Lower Panel*). The green bands show the 65% and 95% confidence intervals for the COMPOSITE sample. The red bands show the 65% and 95% confidence intervals obtained using mock COMPOSITE catalogues based on FLRW redshifts corrected by the local boost of 635 km/s. The purple bands show the 65% and 95% confidence intervals for mock FLRW catalogues with a 350 km/s boost in the same direction.

4. We construct 100,000 mock catalogues, using the known uncertainties. Firstly, each boosted redshift in step 3 is drawn randomly from a Gaussian distribution taking into account the uncertainties in (2.5) and (2.6). Secondly, in step 1 each distance from the COMPOSITE sample is replaced with a distance $d_{\mathcal{N}}$

$$d_{\mathcal{N}} = \mathcal{N}(\mu = d_i, \sigma = \Delta d_i) \tag{3.16}$$

equal to a random number drawn from a Gaussian distribution whose mean value is d_i with standard deviation equal to each individual distance uncertainty, Δd_i.

5. For each of these mock catalogues we calculate the Hubble expansion and its anisotropy as outlined in Sec. 3.1.

The results are presented in Fig. 3. As seen the anisotropy produced by a FLRW model with local boost is characterized by a dipole three times larger than is observed in the COMPOSITE data at low redshift, and differs by more than 2σ for all redshifts $z <$

– 13 –

0.04. On the other hand the quadrupole generated by the FLRW model with local boost is comparable to that of the COMPOSITE sample as $z \to 0$, but becomes smaller than that of the COMPOSITE sample for $z \gtrsim 0.01$, being consistent with that of the randomly reshuffled data in Fig. 2. Thus for $z > 0.01$ the local boost of 635 km/s cannot account for the amplitude of the observed quadrupole in the COMPOSITE sample.

We note that the linear $\cos\theta$ dependence in (3.15) gives rise to a pure dipole anisotropy at fixed values of z_{FLRW} and d_L in a linear Hubble relation. However, once (3.15) is substituted in the Taylor series (3.3), a quadrupole and higher order multipoles are also generated at fixed redshift. The amplitude of the boosted quadrupole in Fig. 3 is larger than would be produced with perfect data, the ratio of the boost quadrupole and dipole contributions to (3.12) generated by (3.3) and (3.15) being proportional to $\beta_o{}^2 \sim 4 \times 10^{-6}$. The relatively large value of the ratio $C_2/C_1 \sim 0.05$ reflects the combination of the effect of angular smoothing in the Gaussian window average (3.7)–(3.9) with the actual distance uncertainties assigned to the mock data, leading to $C_2 \sim 0.004$ at low redshift for the randomly reshuffled COMPOSITE data in Fig. 2.

We have investigated by how much the magnitude of the local boost on the axis of the CMB and LG frames must be reduced in order to match the Hubble expansion dipole of the COMPOSITE sample. We find that a 350 km/s boost would match the Hubble expansion dipole, giving results which are also shown in Fig. 3. The quadrupole of the COMPOSITE sample is not matched, however. For a 350 km/s boost the quadrupole is consistent with the residual level of the randomly reshuffled data within 2σ for all redshifts.

The interpretation of the anisotropy within a framework of the FLRW model plus local boosts leads to a conundrum. The mismatch between the 350 km/s amplitude of a Local Group boost that would be consistent with the Hubble dipole anisotropy and the 635 km/s boost required to account for the CMB dipole kinematically suggests two possible solutions: (i) the galaxies in the COMPOSITE sample are in a coherent bulk flow with respect to the CMB on scales up to $z \sim 0.045$; or (ii) the Hubble dipole and other anisotropies contain a substantial nonkinematic component.

While the bulk flow hypothesis is the one that is widely studied — being based on the standard FLRW model — it is at odds with the results of [45] that the spherically averaged, or monopole, Hubble expansion variation is very significantly reduced in the LG frame as compared to the CMB frame on $\lesssim 70\,h^{-1}$Mpc scales. The spherical average of a coherent bulk flow on such scales does not produce a monopole expansion variation of the character seen in the COMPOSITE sample [45], and such a result is not seen in N–body Newtonian simulations[7]. Moreover, the signature of a systematic boost offset (2.8) from the LG to CMB frame is seen in both the COMPOSITE and Cosmicflows-2 samples [46], providing a potential explanation for the CMB frame monopole variation if the LG rest frame is closer to being the frame in which anisotropies in the Hubble expansion are minimized.

We will now investigate the extent to which a nonkinematic interpretation of the anisotropies is observationally consistent by ray tracing in exact inhomogeneous solutions of the Einstein equations.

---

[7]The effect of a local boost of the central observer is the most significant aspect of our analysis. FLRW models with additional inhomogeneities produced by Newtonian N–body simulations do not lead to results significantly different from a pure FLRW model plus local boost shown as shown in Fig. 3. These results will be reported elsewhere [72].

4 Light propagation in the non-linear relativistic regime and the origin of anisotropies

Relativistic cosmological models predict the expansion of the Universe, which induces cosmological redshift. Cosmic expansion, however, does depend on the local coupling of matter and curvature, and only in the FLRW model is expansion spatially homogeneous and isotropic. The general relativistic formula for the redshift is [81]

$$\frac{1}{(1+z)^2}\frac{\mathrm{d}z}{\mathrm{d}s} = \frac{1}{3}\Theta + \Sigma_{ab}n^a n^b + u^a{}_{;b}u^b n_a, \tag{4.1}$$

where u^a is the matter velocity field, n_a is the connecting covector field locally orthogonal[8] to u^a, Σ_{ab} is the shear of the velocity field, and $\Theta = u^a{}_{;a}$ is its expansion. In the limit of spatially homogeneous and isotropic models the shear vanishes, $\Sigma_{ab} \to 0$, and the expansion of the velocity field reduces to the Hubble parameter, $\Theta \to 3H(t)$. However, once cosmic structures form, the expansion field becomes non-uniform (ranging from $\Theta = 0$ inside virialized clusters of galaxies to $\Theta > 3H_0$ within cosmic voids), and so the shear, Σ_{ab}, and acceleration, $u^a{}_{;b}u^b$, of the velocity field are nonzero.

Distances are also affected by presence of cosmic structures. The general relativistic framework that allows us to calculate the distance is based on the Sachs equations [82, 83]

$$\frac{\mathrm{d}^2 d_A}{\mathrm{d}s^2} = -\left(\sigma^2 + \frac{1}{2}R_{ab}k^a k^b\right)d_A, \tag{4.2}$$

where k^a is the tangent to null geodesics in a congruence, $\sigma = \frac{1}{2}\sigma_{ab}\sigma^{ab}$ is the scalar shear of the null geodesic bundle, and R_{ab} is the Ricci curvature. The first term on the right hand side of (4.2) is often referred to as the Weyl focusing as it involves the Weyl curvature, while the second term is known as the Ricci focusing. For the type of inhomogeneities considered in this paper, the amplitudes of the density contrast and density gradient are such that the Weyl focusing is negligibly small compared to the Ricci focusing [84]. Therefore, in this paper we work within the Ricci focusing regime[9] and we neglect any contribution from σ. The luminosity distance d_L is then given by the reciprocity theorem [81, 85]

$$d_L = (1+z)^2 d_A. \tag{4.3}$$

Solving (4.2), (4.3) for the areal and luminosity distances, and (4.1) for the redshift, we arrive at a general relativistic distance–redshift relation, which will give rise to an anisotropic Hubble expansion generated by the spatial inhomogeneities in the geometric terms on the right hand sides of (4.1) and (4.2). The anisotropies will be most prominent over length scales characteristic of the matter inhomogeneities, and will have characteristics which are distinct from a simple FLRW geometry plus Lorentz boosts.

4.1 The geometry and Einstein equations

In order to solve (4.1), (4.2) for the distance–redshift relation we need to calculate all relevant physical quantities such as the Ricci curvature, the shear of the null and timelike geodesic

---

[8]I.e., $u^a n_a = 0$, $n_a n^a = 1$. In the case that the vorticity of the velocity field vanishes — i.e., $u_{[a;b]} = 0$ — then n_a is also the normal to a spatial hypersurface with tangent u^a. For practical purposes, this is taken to be the case in cosmological averages.

[9]See ref. [84] for a detailed discussion on the applicability of Ricci focusing and the contribution of the Weyl curvature on light propagation.

bundles, and the expansion scalar. For this purpose we use the Szekeres solution [16], which is the most general known exact solution of the Einstein equations for an inhomogeneous dust source. In the limit of a spatially homogeneous matter distribution it reduces to the FLRW model.

The advantage of the Szekeres model over the perturbed FLRW model[10] is that we can account for possible nonkinematic differential expansion which we find to be associated with actual observed structures in the local Universe. In particular, we will study a quasispherical Szekeres model generated by a spherical void onto which an additional inhomogeneity with an axial density gradient is superposed. Thus we have both overdense and underdense regions in the same exact solution of Einstein's equations.

The Szekeres model reduces to the spherically symmetric LT model in the limit of no superposed axial density gradient. In the LT limit the anisotropy in the Hubble expansion is generated solely by the off–centre position of an observer relative to the centre of the inhomogeneity. In the Szekeres model this parameter will still play a role. However, the angle between the observer and the density gradient axis will also give rise to more complex and realistic anisotropies than are possible with the LT model alone. This allows us greater freedom to more closely model actual structures in the local Universe. Of course, the Szekeres model still has limitations as to what it can describe. (We will return to this issue later on.)

The metric of the quasispherical Szekeres solution [16, 86] is usually represented in the following form

$$ds^2 = c^2 dt^2 - \frac{\left(R' - R\frac{\mathcal{E}'}{\mathcal{E}}\right)^2}{1 - k} dr^2 - \frac{R^2}{\mathcal{E}^2}(dp^2 + dq^2), \tag{4.4}$$

where $' \equiv \partial/\partial r$, $R = R(t, r)$, and $k = k(r) \leq 1$ is an arbitrary function of r. The function $\mathcal{E}$ is given by

$$\mathcal{E}(r, p, q) = \frac{1}{2S}(p^2 + q^2) - \frac{P}{S}p - \frac{Q}{S}q + \frac{P^2}{2S} + \frac{Q^2}{2S} + \frac{S}{2}, \tag{4.5}$$

where the functions $S = S(r)$, $P = P(r)$, $Q = Q(r)$, but are otherwise arbitrary. We take the coordinates r, p, q and the functions P, Q, R, S, $\mathcal{E}$ all to have dimensions of length. We can also define angular coordinates, (θ,ϕ), by

$$p - P = S \cot \frac{\theta}{2} \cos \phi, \qquad q - Q = S \cot \frac{\theta}{2} \sin \phi. \tag{4.6}$$

Then $\mathcal{E} = S/(1 - \cos\theta)$, and the metric (4.4) takes the form

$$ds^2 = c^2 dt^2 - \frac{1}{1-k}\left[R' + \frac{R}{S}\left(S' \cos\theta + N \sin\theta\right)\right]^2 dr^2 - \left[\frac{S' \sin\theta + N\left(1 - \cos\theta\right)}{S}\right]^2 R^2 dr^2$$

$$- \left[\frac{(\partial_\phi N)\left(1 - \cos\theta\right)}{S}\right]^2 R^2 dr^2 + \frac{2\left[S' \sin\theta + N\left(1 - \cos\theta\right)\right]}{S} R^2 dr\, d\theta$$

$$- \frac{2(\partial_\phi N)\sin\theta\left(1 - \cos\theta\right)}{S} R^2 dr\, d\phi - R^2(d\theta^2 + \sin^2\theta\, d\phi^2), \tag{4.7}$$

where $N(r, \phi) \equiv (P' \cos\phi + Q' \sin\phi)$.

The Einstein equations with cosmological constant, Λ, and dust source of mass density, ρ,

$$G_{ab} - \Lambda g_{ab} = \kappa^2 \rho\, u_a u_b, \tag{4.8}$$

---

[10]We will present a comparison of the distinct differences from N–body simulations in a future paper [72].

where $\kappa^2 = 8\pi G/c^4$, reduce to the evolution equation and the mass distribution equation. The evolution equation is

$$\dot{R}^2 = -k(r) + \frac{2M(r)}{R} + \frac{1}{3}\Lambda c^2 R^2, \tag{4.9}$$

where $\dot{} \equiv \partial/\partial t$, and $M(r)$ is a function related to the mass density by

$$\kappa\rho = \frac{2\left(M' - 3M\mathcal{E}'/\mathcal{E}\right)}{R^2\left(R' - R\mathcal{E}'/\mathcal{E}\right)}. \tag{4.10}$$

Note that

$$\frac{\mathcal{E}'}{\mathcal{E}} = \frac{-1}{S}\left[S'\cos\theta + N\sin\theta\right] \tag{4.11}$$

is the only term in (4.10) which gives a departure from spherical symmetry. One is free to specify the various functions as long as (4.9)–(4.11) are satisfied. Since $R(t, r)$ is the only function that depends on time, (4.9) can be integrated to give

$$t - t_B(r) = \int\limits_0^R \frac{\mathrm{d}\widetilde{R}}{\sqrt{-k + 2M/\widetilde{R} + \frac{1}{3}\Lambda c^2 \widetilde{R}^2}}, \tag{4.12}$$

where $t_B(r)$ is one more arbitrary function called the *bang time* function, which describes the fact that the age of the Universe can be position dependent. If we demand that the age of the Universe is everywhere the same for comoving observers — the homogeneous Big Bang condition — then the above equations link $M(r)$ and $k(r)$. In the generic case M and k can be arbitrary, which could mean either a non-uniform Big Bang, or some turbulent initial conditions; i.e., conditions that would require a more complicated model than the Szekeres model.

The matter distribution in the Szekeres model has a structure of a dipole superposed on a monopole, (cf., upper left panel of Fig. 4). In order to determine the Szekeres model and solve all the equations, we need to specify its five arbitrary functions. These are: M and k which describe the monopole distribution, and S, P, and Q which describe the dipole. If S, P, Q are constant the dipole vanishes and we recover spherical symmetry; if $S' \neq 0$, and $P' = 0 = Q'$ then the model is axially symmetric. These five functions (or any other combination of functions from which these can be evaluated) are sufficient to solve all the equations that describe the evolution of matter and light propagation in the evolving geometry.

In the FLRW limit when the model becomes spatially homogeneous and isotropic we have:

$$R \to ra(t) \tag{4.13}$$
$$M \to M_0 r^3, \tag{4.14}$$
$$k \to k_0 r^2, \tag{4.15}$$

where $M_0 = \frac{1}{2}H_0^2\Omega_m$, $k_0 = H_0^2(\Omega_m + \Omega_\Lambda - 1)$, and the functions S, P, and Q are constant ($S' = 0 = P' = Q'$). Therefore, in the FLRW limit the dependence on r in (4.9) cancels out and after dividing by a^2 we recover the well known form of the Friedmann equation

$$H^2 = H_0^2\left(\Omega_m a^{-3} + \Omega_k a^{-2} + \Omega_\Lambda\right),$$

where $\Omega_\Lambda = \Lambda c^2/(3H_0^2)$, and $\Omega_m + \Omega_k + \Omega_\Lambda = 1$.

Let us then model the departure from homogeneity using the following profile of the mass function

$$M = M_0 r^3 \left[1 + \delta_M(r)\right], \tag{4.16}$$

where

$$\delta_M(r) = \frac{1}{2}\delta_0 \left(1 - \tanh\frac{r - r_0}{2\Delta r}\right), \tag{4.17}$$

with $-1 \leq \delta_0 < 0$, is a localized perturbation which is underdense at the origin. As $r \to \infty$, we have $\delta_M \to 0$ so that the spatial geometry is asymptotically that of the homogeneous and isotropic FLRW model. We normalize this geometry by choosing the spatially flat FLRW model which best fits the Planck satellite data, with $\Omega_m = 0.315$ and $H_0 = 67.3\,\mathrm{km\,s^{-1}\,Mpc^{-1}}$ [79].

The function $k(r)$ is then evaluated from (4.12) for each r under the assumptions: (i) the age of the Universe is everywhere the same for comoving observers, $t_B = 0$; and (ii) $R(t_0, r) = r$ for each r, where the age of the Universe, t_0, is equal to that of the asymptotic background spatially flat FLRW model.

Finally we assume axial symmetry, with dipole described by only the function S, which we choose to be:

$$\begin{aligned} S &= r\left(\frac{r}{1\ \mathrm{Mpc}}\right)^{\alpha-1}, \\ P &= 0, \\ Q &= 0, \end{aligned} \tag{4.18}$$

where α is a free parameter. When $\alpha \to 0$ the model becomes the spherically symmetric LT model, as shown in the lower left panel of Fig. 4.

The model has 7 free parameters:

- 4 parameters that specify the Szekeres model α, δ_0, r_0, Δr,

- 3 parameters that specify the position of the observer r_{obs}, φ_{obs}, ϑ_{obs}.

Since the model considered here is axially symmetric, we can choose the observer to lie in the plane $\varphi_{\mathrm{obs}} = \pi/2$ without loss of generality. In order to reduce the dimension of the parameter space we also set $\Delta r = 0.1r_0$ for simplicity. That leaves us with 5 parameters. In reality, we expect the perturbations that describe actual cosmic structures to be much more complicated than the parameterization adopted here. So while this gives us some flexibility, not all structures can be described using this parameterization. The structures that can be described using this parameterization consist of a void and an adjacent overdensity, as presented in the upper left panel of Fig. 4. While not perfect, this parameterization aims to model some of the major structures in the local Universe, such as the Local Void and the overdensity known as the Great Attractor [66].

By varying the five free parameters, we can tune the size of the void and/or overdensity, the amplitude of the density contrast and the position of the observer relative to the structures. We run a search through this 5-dimensional parameter space looking for a model which as closely as possible satisfies constraints in the following order of importance:

1. The CMB temperature has a maximum value of $T_0 + \Delta T$ relative to the mean $T_0 = 2.725\,\text{K}$, where

$$\Delta T(\ell = 276.4°, b = 29.3°) = 5.77 \pm 0.36 \text{ mK}, \qquad (4.19)$$

   which corresponds to the CMB temperature dipole amplitude and direction in the LG rest frame.

2. The quadrupole of the CMB anisotropy is lower than the observed value [87]

$$C_{2,\text{CMB}} < 242.2^{+563.6}_{-140.1} \ \mu\text{K}^2. \qquad (4.20)$$

   While the dipole of the CMB is significantly affected by local expansion, the quadrupole is dominated by the baryonic physics of the early Universe, and the observed value itself is about 5 times smaller than the expectation based on the standard cosmology. Therefore we implement this constraint to ensure that the quadrupole generated by local inhomogeneities is much lower than the quadrupole generated at last scattering.

3. The dipole of the Hubble expansion anisotropy and its redshift dependence must be consistent with the observed anisotropy of the COMPOSITE sample as presented in Fig. 3.

4. The quadrupole of the Hubble expansion anisotropy and its redshift dependence must be consistent with the observed anisotropy of the COMPOSITE sample as presented in Fig. 3.

4.2   Constructing mock catalogues

The algorithm of our analysis can be summarized by the following steps:

1. We first specify the Szekeres model.

2. We apply the HEALPix grid of the sky and propagate light rays in these directions.

3. We then calculate the CMB temperature maps.

4. We use HEALPix routines to calculate the anisotropy of the CMB map.

5. We take the COMPOSITE sample. For each galaxy we have its angular position (ℓ_i, b_i), luminosity distance d_i, uncertainty in distance Δd_i and redshift z_i. For each of these directions (ℓ_i, b_i) we numerically propagate light rays, using the null geodesic equations of the Szekeres model, up until $d = d_i$. We then write down the redshift evaluated within the Szekeres model z_{Sz}.

6. We construct the mock COMPOSITE catalogue, by replacing z_i with z_{Sz}, (i.e., the redshift obtained in the Szekeres model for this direction and this distance).

7. We construct 100,000 mock catalogues, by taking into account the actual uncertainties, Δd_i, in the distances. As for the boosted FLRW mock catalogues, this is done by replacing the distance from the COMPOSITE sample by $d_{\mathcal{N}}$ according to (3.16).

8. For each of these mock catalogues we calculate the Hubble expansion and its anisotropy as outlined in Sec. 3.1.
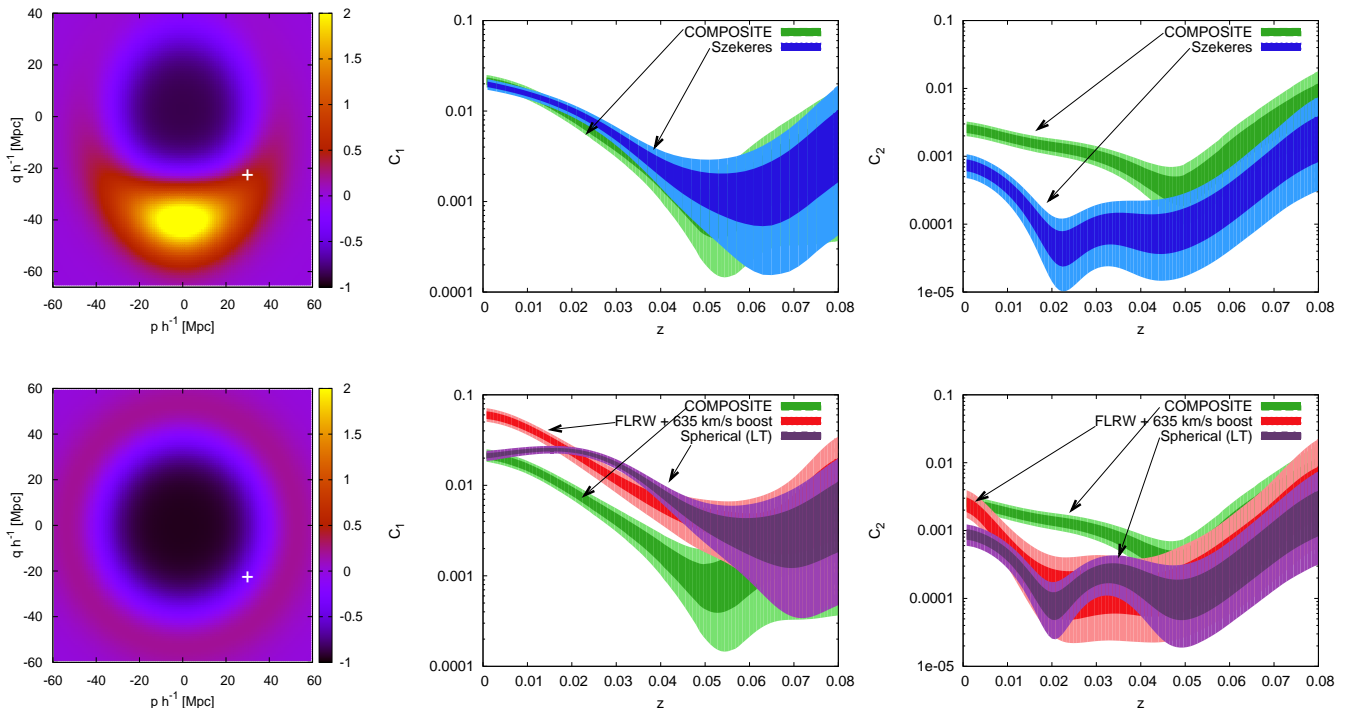
Figure 4. The anisotropy of the Hubble expansion. *Upper Panels* show the anisotropy of the Hubble expansion within the Szekeres model, whose density distribution is presented in the upper left panel (this panel shows the density contrast, $\delta_\rho = (\rho - \bar{\rho})/\bar{\rho}$ given in the right hand scale, when smoothed with Gaussian kernel of size $8\,h^{-1}$Mpc); the position of the observer is marked with a cross "+". *Lower Panels* show the anisotropy of the Hubble expansion within the spherical model (LT) model, whose density distribution is presented in the lower left panel (cross "+" marks the position of the observer); the anisotropy of the Hubble expansion evaluated within the FLRW model with a local boost of 635 km/s is also presented for comparison. This shows how important matter anisotropies are to fully account for the observed anisotropies of the Hubble expansion.

4.3 Anisotropy of the Hubble expansion generated by cosmic structures modelled by the Szekeres model

Our search through the 5-dimensional parameter leads us to a model, whose mass profile as well as the position of the observer are presented in the upper left panel of Fig. 4. The values of the free parameters are

$$
\begin{aligned}
\alpha &= 0.86, \\
\delta_0 &= -0.86, \\
r_0 &= 38.5 \ h^{-1} \ \text{Mpc}, \\
\Delta r &= 3.85 \ h^{-1} \ \text{Mpc},
\end{aligned}
\tag{4.21}
$$

and the position of the observer:

$$r_{\mathrm{obs}} = 25 h^{-1} \text{ Mpc},$$
$$\varphi_{\mathrm{obs}} = 0.5\pi,$$
$$\vartheta_{\mathrm{obs}} = 0.705\pi. \tag{4.22}$$

These distances are coordinate distances, not radial proper distances or luminosity distances.

Interestingly, if we take the region of maximum overdensity in Fig. 4, with density contrast $\delta\rho/\rho > 2$, this region is found to be located at redshifts and luminosity distances in the ranges $0.003 \lesssim z \lesssim 0.013$ and $16\,h^{-1} \lesssim D_L \lesssim 53\,h^{-1}\text{Mpc}$, comparable to those of the Centaurus cluster / Great Attractor[11]. We did not supply the redshift of the overdensity as an *a priori* constraint, but arrived at it using a grid search on possible Szekeres models following the criteria specified above.

Furthermore, in terms of the angular extent, the region with $\delta\rho/\rho > 2$ occupies an ellipsoidal region with $220° < \ell < 320°$, and $-60° < b < 40°$. The Centaurus cluster at $(\ell, b) = (302.4°, 21.6°)$ on the near side of the Great Attractor is thus contained with the overdense region. However, the Norma cluster at $(\ell, b) = (325.3°, -7.3°)$ which is in the angular centre of the Great Attractor, but on the far side in distance at $z = 0.0141 \pm 0.0002$ in the LG frame falls 5° outside our overdense region by angle and $\Delta z = 0.0011$ by redshift. The fact that the alignment of the overdensity is very close to the actual Great Attractor, but does not yet match precisely is consistent with the fact that there are further features of the Hubble expansion that we have still to account for – its quadrupole – as we shall discuss below.

The anisotropy of the Hubble expansion within such a model is presented in the upper panels of Fig. 4. We find that the first three criteria given in Sec. 4.2 are all satisfied. In particular, the CMB temperature dipole is

$$\Delta T_{\mathrm{CMB}} = 5.58 \text{ mK},$$

as is expected in the LG frame, while the quadrupole of the CMB temperature anisotropy is

$$C_{2,\mathrm{CMB}} = 8.26 \ \mu\text{K}^2.$$

Furthermore, the dipole of the Hubble expansion within this model is consistent with the dipole of the Hubble expansion inferred from the COMPOSITE sample.

The results shown in Fig. 4 display the clear advantage of the Szekeres model in comparison with a FLRW model plus local boosts, as discussed in Sec. 3.3. Applying a local boost to an otherwise homogeneous and isotropic universe we found that it was not possible to fit the Hubble expansion dipole and the CMB temperature dipole simultaneously. By contrast the Szekeres model simultaneously matches both the CMB temperature dipole in the LG frame and the Hubble expansion dipole of the COMPOSITE sample over all redshifts in the survey with sufficient data. Given the fact that the structure of the Universe on scales below $100\,h^{-1}\text{Mpc}$ is very inhomogeneous, and that differential cosmic expansion is a generic feature of cosmological solutions of Einstein's equation, it should perhaps not be a surprise that the inhomogeneous model performs better.

---

[11]The Centaurus cluster, at LG frame redshift of $z = 0.0104 \pm 0.0001$ [88], lies in the nearer portion of the Great Attractor region [89].

On the other hand, the particular Szekeres model considered here is not able to reproduce the quadrupole of the Hubble expansion seen in the COMPOSITE sample, which is about three times larger in magnitude than in the simulation. The Hubble expansion quadrupole in the Szekeres model (4.16)–(4.22) in fact has an amplitude consistent with that of the randomly reshuffled data in Fig. 2, and is not statistically significant.

The fact that we can account for the Hubble expansion dipole, but not the quadrupole may well be due to the simplicity of the model (4.16)–(4.22), (cf., upper panel of Fig. 4). In particular, the choice (4.18) enforces an axial symmetry on the mass distribution, which could be altered to give finer details. This would require a more complex model, and is left for future investigations.

As an indication of how the properties of the Hubble expansion variation are induced by changes in the matter distribution, we have also investigated the anisotropy of the Hubble expansion evaluated using a spherical void LT model, which is obtained from the Szekeres model in the limit of a vanishing matter dipole, $\alpha \to 0$.

We use the same parameterization and procedure as outline above with $\alpha = 0$, which ensures spherical symmetry. As in the case of a simple boost (Sec. 3.3) we are not able to simultaneously fit the CMB temperature variation and the full redshift dependence of the Hubble expansion anisotropy. At best, we can only reproduce some of the features.

An example of this investigation is presented in lower panels of Fig. 4. The values of the free parameters are

$$\begin{aligned}
\alpha &= 0, \\
\delta_0 &= -0.95, \\
r_0 &= 45.5 \ h^{-1} \ \mathrm{Mpc}, \\
\Delta r &= 4.55 \ h^{-1} \ \mathrm{Mpc}
\end{aligned} \tag{4.23}$$

and the position of the observer is

$$\begin{aligned}
r_{\mathrm{obs}} &= 28 h^{-1} \ \mathrm{Mpc}, \\
\varphi_{\mathrm{obs}} &= 0.5\pi, \\
\vartheta_{\mathrm{obs}} &= 0.5\pi.
\end{aligned} \tag{4.24}$$

The model matches the correct temperature dipole of the CMB in the LG frame

$$\Delta T_{\mathrm{CMB}} = 5.63 \ \mathrm{mK}$$

and the quadrupole of the CMB temperature anisotropy is

$$C_{2,\mathrm{CMB}} = 20.73 \ \mu\mathrm{K}^2.$$

However, the Hubble expansion dipole anisotropy can only be matched at very low redshifts (see middle panel of Fig. 4). As the redshift is increased the magnitude of the dipole increases until for, $z > 0.015$, it becomes consistent with that predicted by the FLRW model plus a local boost of 635 km/s in the LG frame — which was not consistent with the COMPOSITE data, however.

This illustrates the fact that the amplitudes of the CMB dipole and higher multipoles in LT models can be roughly estimated for off–centre observers by an effective Newtonian approximation [52] using the velocity appropriate to a boosted observer in the FLRW geometry. This limit was discussed by Wiltshire et al. [45], who gave an example of a LT void

with a somewhat different mass profile but with similar parameters, being 18% larger but with a less sharp density gradient.

An examination of the density profile panels of Fig. 4 illustrates the role that is played by differential cosmic expansion. In particular, Lorentz boosts represent a point symmetry in the tangent space of any general observer. In the case of the LT model, the axis which joins the centre of the void to the position of the off–centre observer defines a direction along which a radial boost can be taken to act from the void centre. Since the differential expansion is purely radial with respect to the centre, it still somewhat mimics the action of a point symmetry. Thus it is not surprising that the LT dipole becomes equivalent to the FLRW model plus boost on scales larger than $r_0 + r_{obs}$. By contrast, the Szekeres model incorporates a mass dipole on an axis distinct from that joining r_0 to r_{obs}. This distributed density gradient therefore gives rise to a differential cosmic expansion which cannot be mimicked by a boost or any other point symmetry relative to the central point, r_0.

The models considered in this Section show how the presence of cosmic structures affect the anisotropy of the Hubble expansion. The more structures that are present in the model, the better is the consistency with observational data.

5 Potential impact on CMB anomalies

Any model cosmology in which (2.3) is nonzero will demand a different to standard approach to the analysis of large angle CMB anisotropies. The multipole expansion of (2.3) will consist of terms which could be deemed to be "anomalous multipoles" relative to the kinematic expectation. As the dipoles will not cancel perfectly, to leading order there will generally be an "anomalous dipole" which may demand a reexamination of the observed power asymmetry and related large angle anomalies [42, 43]. This would have a major impact on observational cosmology, as has already been discussed by Wiltshire et al. [45].

While one should naturally be sceptical of any suggestion that large angle CMB anomalies result from a nonkinematic relativistic differential expansion on $\lesssim 70\,h^{-1}$Mpc scales, a very important implication of the present paper is that ray-traced exact solutions similar to those described here will provide, for the first time ever, concrete models that can actually be tested against Planck satellite data for their effect on large angle anomalies. Such a project might even demand subtle changes in the treatment of the galactic foreground in the map making procedures. Thus it is important to first have the best possible model of relativistic differential expansion before embarking on such a challenge.

A detailed analysis of the multipoles of (2.3) is therefore left for future work. In particular, we need to first refine the Szekeres model to incorporate additional structures giving a Hubble expansion quadrupole with the observed redshift dependence. Since the CMB quadrupole for the Szekeres model (4.21), (4.22) is 30 times smaller in amplitude than the observed CMB quadrupole, we should reasonably expect that this can be accommodated. The redshift dependence of the Hubble expansion dipole and quadrupole seen in the COMPOSITE sample should also to be confirmed with other data sets[12].

In this paper, we have considered LT and Szekeres models in the the LG frame treated as the average isotropic expansion frame, with a ray-traced CMB treated according to (2.4), as this is computationally simpler. With a refined Szekeres model one should also boost to the heliocentric frame and constrain the ray traced simulations with the complete sky map

---

[12]In the case of the Cosmicflows-2 sample [76], for example, this requires a careful treatment of Malmquist biases to remove a monopole bias [30, 46].

of the observed heliocentric dipole from Planck satellite data with an appropriate galactic sky mask applied, rather than adopting our simpler procedure (4.19) of just matching the amplitude of the equivalent temperature dipole in the LG frame.

While one cannot know the outcome of any such simulations before performing them, there are as yet no obstacles to the possibility that such investigations will result in observationally consistent alternative models of the large angle CMB sky. In particular, as was discussed in ref. [45], the claim of the Planck team [90] that the kinematic nature of the transformation from the heliocentric to CMB frames has been verified by the effects of frequency modulation and aberration in the CMB anisotropy spectrum actually depends on angular scale. The boost direction coincides with the expected direction $(\ell, b) = (264°, 48°)$ only for small angle multipoles $l_{\min} = 500 < l < l_{\max} = 2000$. For large angle multipoles $l < l_{\max} = 100$ the inferred boost direction moves across the sky to coincide with the modulation dipole anomaly direction [39], $(\ell, b) = (224°, -22°) \pm 24°$. Since the nonkinematic terms in (2.3) will only affect large angle power, this angular scale dependence of the results of [90] and their association with the anomaly direction is perhaps suggestive.

6 Conclusion

Cosmic structures such as voids, sheets, filaments, and knots participate differently in the expansion of the Universe. The expansion rate gradually changes from no expansion inside virialized high density regions such as superclusters to a higher than average expansion rate inside voids. This differential expansion of the space can be observed in the anisotropy of the Hubble expansion, especially on scales up to a few hundreds megaparsecs. In general relativity, differential cosmic expansion is the norm in all cosmological models which are not spatially homogeneous and isotropic. The anisotropy of the Hubble expansion is thus expected to quantitatively differ from that of a FLRW model in which all departures from homogeneity can be described by local Lorentz boosts of the source and observer.

The effects that we consider in this paper appear to have been largely overlooked as serious possibilities in the past for two reasons. Firstly, in considering nonlinear anisotropies many cosmologists typically think about the Rees–Sciama effect [91], in which one considers a photon traversing *from one average position across a nonlinear structure to another average position*. Such considerations miss the peculiar potential effect of placing observers deep inside the nonlinear structures (cf. Fig. 6 in ref. [56]). When we take the same structures studied in this paper and place observers far from the structures then the amplitude of the temperature anisotropies is of order $|\Delta T|/T < 3 \times 10^{-7}$ consistent with previous estimates which use larger voids and generate a somewhat larger amplitude [92, 93].

Secondly, simple order of magnitude estimates suggest that a Rees–Sciama dipole will in general generate a Rees–Sciama quadrupole of similar order [94], and one might naïvely assume that similar arguments apply to all general nonlinear distance–redshift anisotropies. However, our results show again that one cannot extrapolate the argument for the Rees–Sciama effect involving both a source and observer far from a structure to the case of an observer inside the structure. While it is certainly possible that the relative size of the CMB quadrupole and dipole would be comparable at certain locations in other structures, we find that for observers placed at any position in the Szekeres model (4.21), (4.21) the quadrupole is always much smaller than the bound (4.20). Thus when one is dealing with observers inside a nonlinear structure the details of the density profile and the observer's position are crucially important. In our case, we have a *particular location* relative to structures such as

the Local Void and the "Great Attractor". Our study is the first to benefit from constraining ray tracing simulations with actual large galaxy surveys outside a framework of the FLRW cosmology plus local boosts.

In this paper we investigated the anisotropy pattern of the Hubble expansion, considering the dipole and quadrupole variations in the LG frame. Most previous studies have either focused on the monopole, i.e., the global (average) value of H_0, or on bulk flows. In a way this is analogous to studies of the CMB in 1970s–1990s. However, with increasing amount of data and precision of measurements, we are slowly arriving at the stage where we can study anisotropies of the Hubble expansion, just as we now study the anisotropy of the CMB temperature fluctuations.

In analogy to CMB temperature fluctuations, we show that the Hubble expansion can be decomposed using spherical harmonics and expressed in terms of an angular power spectrum. Moreover, by averaging data at various redshifts we can have additional information about the redshift dependence of the multipoles of the Hubble expansion. Irrespective of any theoretical assumptions about cosmic expansion, this is a novel technique that carries complimentary if not additional information to studies of bulk flow that have been extensively carried out in the past years.

In Sec. 3.1 we developed the formalism used to study the anisotropy of the Hubble expansion. When applied to the COMPOSITE sample we identified the presence of dipole and quadrupole anisotropies in the Hubble expansion. These anisotropies are statistically significant in the data up to $z \lesssim 0.045$. For larger redshifts the amount of data is small and the signal is no longer distinguishable from noise.

We compared the measured anisotropy with predictions from a FLRW model assumed to be homogeneous and isotropic in the CMB frame, and also particular LT and Szekeres models with small scale inhomogeneities in the LG frame. All models were assumed to be identical to a spatially flat FLRW models on scales $\gtrsim 100\,h^{-1}\mathrm{Mpc}$, with parameters fixed to those of the FLRW model that best fits the Planck satellite data [79]. The FLRW model with a local boost from the CMB to LG frame did not fit the observed redshift dependence of the dipole of the Hubble expansion of the COMPOSITE sample as seen in the LG frame. In order to match the observed features of the dipole of the Hubble expansion, the local boost would have to be reduced to approximately 350 km/s, which is much smaller than the actual 635 ± 38 km/s that is required if the CMB temperature dipole is purely kinematic.

A quasispherical Szekeres solution that allows for variations of the local geometry generated by the presence of cosmic structures, which effectively model the Local Void and "Great Attractor", was found to improve the fit. This analysis shows that the local cosmological environment does affect the Hubble expansion. Physically, this can be understood in terms of the differential expansion of the space, with the void expanding faster and the overdensity expanding at a slower than the average expansion rate.

As yet, the numerical model does not have a Hubble quadrupole as large as that seen in the COMPOSITE sample. However, if extra modifications are added — for example, by using methods to include extra structures [65] — then given the magnitude of the effects that remain to be explained, it is highly plausible that highly accurate models of the local cosmic expansion can be developed.

All our models are constrained by a match to the magnitude and direction of the CMB temperature dipole. Since the models are nonlinear the addition of further structures can affect the alignment and scale of the structures, and the position of the observer, as compared to a simpler model. In moving from the simple LT void model to our single void / single

overdensity Szekeres model, for example, the scale of the void was reduced by 40%, while also achieving a fit to the Hubble expansion dipole over a range of redshifts.

The effect which remains to be explained – the Hubble expansion quadrupole – is an order of magnitude smaller than the Hubble expansion dipole. Therefore we should not expect such large changes of scale as occurred between the LT and Szekeres models already studied. However, we note that the overdensity in our simple Szekeres model overlaps with the observed Great Attractor in both angle and redshift on the near side but not completely on the far side. Furthermore, the additional major structures that should still be accounted for include most notably the Perseus–Pisces concentration, which lies at LG frame redshifts 0.0182–0.0194. This is at the upper end of the redshift/distance range of the structures that we are considering, with a a likely impacting on the alignment of the far side of the overdensity which we have identified with the Great Attractor. Whether this can be done while also accounting for the Hubble expansion quadrupole is an important question left for future work.

As discussed in Sec. 5, our approach may potentially provide a simple physical explanation of particular large anomalies in the CMB radiation, in terms of known physics. But this is a matter for future investigations.

The main result of this paper is that with just the FLRW geometry plus a local boost of the Local Group of galaxies it is impossible to simultaneously fit both the CMB dipole and quadrupole anisotropies and the redshift dependence of the dipole anisotropy of the local expansion of the Universe, determined by the COMPOSITE sample. To explain the observed features we need to use models that exhibit differential cosmic expansion. Further refinement of such models may potentially have a major impact on cosmology.

Acknowledgments

References

[1] F. Hoyle and M.S. Vogeley, *Voids in the Point Source Catalogue Survey and the Updated Zwicky Catalog*, *Astrophys. J.* **566** (2002) 641, [`astro-ph/0109357`]

[2] F. Hoyle and M.S. Vogeley, *Voids in the 2dF Galaxy Redshift Survey*, *Astrophys. J.* **607** (2004) 751, [`astro-ph/0312533`]

[3] A.V. Tikhonov and I.D. Karachentsev, *Minivoids in the local volume*, *Astrophys. J.* **653** (2006) 969, [`astro-ph/0609109`]

[4] D.C. Pan, M.S. Vogeley, F. Hoyle, Y.Y. Choi and C. Park, *Cosmic voids in Sloan Digital Sky Survey Data Release 7*, *Mon. Not. Roy. Astron. Soc.* **421** (2012) 926, [`arXiv:1103.4156`]

[5] J.E. Forero–Romero, Y. Hoffman, S. Gottlöber, A. Klypin and G. Yepes, *A dynamical classification of the cosmic web*, *Mon. Not. Roy. Astron. Soc.* **396** (2009) 1815, [`arXiv:0809.4135`]

[6] M. Bilicki, J.A. Peacock, T.H. Jarrett, M.E. Cluver and L. Steward, *Mapping the cosmic web with the largest all-sky surveys*, *IAU Symp.* **308** (2014), [`arXiv:1408.0799`]

[7] J. Einasto, *Yakov Zeldovich and the Cosmic Web Paradigm*, *IAU Symp.* **308** (2014), [arXiv:1410.6932]

[8] D.W. Hogg, D.J. Eisenstein, M.R. Blanton, N.A. Bahcall, J. Brinkmann, J.E. Gunn and D.P. Schneider, *Cosmic homogeneity demonstrated with luminous red galaxies*, *Astrophys. J.* **624** (2005) 54, [astro-ph/0411197]

[9] F. Sylos Labini, N.L. Vasilyev, L. Pietronero and Y.V. Baryshev, *Absence of self-averaging and of homogeneity in the large scale galaxy distribution*, *Europhys. Lett.* **86** (2009) 49001, [arXiv:0805.1132]

[10] M. Scrimgeour, T. Davis, C. Blake, et al., *The WiggleZ Dark Energy Survey: the transition to large-scale cosmic homogeneity*, *Mon. Not. Roy. Astron. Soc.* **425** (2012) 116, [arXiv:1205.6812]

[11] R.G. Clowes, K.A. Harris, S. Raghunathan, L.E. Campusano, I.K. Soechting and M.J. Graham, *A structure in the early universe at $z \sim 1.3$ that exceeds the homogeneity scale of the R-W concordance cosmology*, *Mon. Not. Roy. Astron. Soc.* **429** (2013) 2910, [arXiv:1211.6256]

[12] B.F. Roukema, T. Buchert, J.J. Ostrowski and M.J. France, *Can an inhomogeneous metric be detected with the baryonic acoustic oscillation peak?*, *Mon. Not. Roy. Astron. Soc.* **448** (2015) 1660, [arXiv:1410.1687]

[13] G. Lemaître, *l'Univers en expansion*, *Ann. Soc. Sci. Bruxelles* **A 53** (1933) 51 *The expanding universe*, [English translation: *Gen. Rel. Grav.* **29** (1997) 641]

[14] R.C. Tolman, *Effect of inhomogeneity on cosmological models*, *Proc. Nat. Acad. Sci.* **20** (1934) 169

[15] H. Bondi, *Spherically symmetrical models in general relativity*, *Mon. Not. Roy. Astron. Soc.* **107** (1947) 410

[16] P. Szekeres, *A class of inhomogeneous cosmological models*, *Commun. Math. Phys.* **41** (1975) 55

[17] J.M. Stewart and D.W. Sciama, *Peculiar velocity of the sun and its relation to the cosmic microwave background*, *Nature* **216** (1967) 748

[18] P.J.E. Peebles and D.T. Wilkinson, *Comment on the anisotropy of the primeval fireball*, *Phys. Rev.* **174** (1968) 2168

[19] R.B. Partridge and D.T. Wilkinson, *Isotropy and homogeneity of the universe from measurements of the cosmic microwave background*, *Phys. Rev. Lett.* **18** (1967) 557

[20] R. Watkins, H.A. Feldman and M.J. Hudson, *Consistently large cosmic flows on scales of $100 h^{-1}$ Mpc: A challenge for the standard ΛCDM cosmology*, *Mon. Not. Roy. Astron. Soc.* **392** (2009) 743, [arXiv:0809.4041]

[21] G. Lavaux, R.B. Tully, R. Mohayaee and S. Colombi, *Cosmic flow from 2MASS redshift survey: The origin of CMB dipole and implications for ΛCDM cosmology*, *Astrophys. J.* **709** (2010) 483, [arXiv:0810.3658]

[22] A. Kashlinsky, F. Atrio–Barandela, H. Ebeling, A. Edge and D. Kocevski, *A new measurement of the bulk flow of X-ray luminous clusters of galaxies*, *Astrophys. J.* **712** (2010) L81, [arXiv:0910.4958]

[23] J. Colin, R. Mohayaee, S. Sarkar and A. Shafieloo, *Probing the anisotropic local universe and beyond with SNe Ia data*, *Mon. Not. Roy. Astron. Soc.* **414** (2011) 264, [arXiv:1011.6292]

[24] A. Nusser and M. Davis, *The cosmological bulk flow: consistency with ΛCDM and $z \approx 0$ constraints on σ_8 and γ*, *Astrophys. J.* **736** (2011) 93, [arXiv:1101.1650]

[25] S.J. Turnbull, M.J. Hudson, H.A. Feldman, M. Hicken, R.P. Kirshner and R. Watkins, *Cosmic flows in the nearby universe from Type Ia Supernovae*, *Mon. Not. Roy. Astron. Soc.* **420** (2012) 447, [arXiv:1111.0631]

[26] G. Lavaux, N. Afshordi, M.J. Hudson, *First measurement of the bulk flow of nearby galaxies using the cosmic microwave background*, Mon. Not. Roy. Astron. Soc. **430** (2013) 1617, [arXiv:1207.1721]

[27] Y.Z. Ma and D. Scott, *Cosmic bulk flows on $50\,h^{-1}Mpc$ scales: A Bayesian hyper-parameter method and multi-shells likelihood analysis*, Mon. Not. Roy. Astron. Soc. **428** (2013) 2017, [arXiv:1208.2028]

[28] F. Atrio–Barandela, *On the statistical significance of the bulk flow measured by the Planck satellite*, Astron. Astrophys. **557** (2013) A116, [arXiv:1303.6614]

[29] Planck Collaboration, P.A.R. Ade, N. Aghanim, M. Arnaud, et al., *Planck intermediate results. XIII. Constraints on peculiar velocities*, Astron. Astrophys. **561** (2014) A97, [arXiv:1303.5090]

[30] Y. Hoffman, H.M. Courtois and R.B. Tully, *Cosmic bulk flow and the local motion from Cosmicflows-2*, Mon. Not. Roy. Astron. Soc. **449** (2015) 4494, [arXiv:1503.05422]

[31] J. Carrick, S.J. Turnbull, G. Lavaux and M.J. Hudson, *Cosmological parameters from the comparison of peculiar velocities with predictions from the 2M++ density field*, Mon. Not. Roy. Astron. Soc. **450** (2015) 317, [arXiv:1504.04627]

[32] M. Tegmark, A. de Oliveira–Costa and A.J.S. Hamilton, *A high resolution foreground cleaned CMB map from WMAP*, Phys. Rev. **D 68** (2003) 123523, [astro-ph/0302496]

[33] H.K. Eriksen, F.K. Hansen, A.J. Banday, K.M. Górski and P.B. Lilje, *Asymmetries in the CMB anisotropy field*, Astrophys. J. **605** (2004) 14 [*Erratum ibid* **609** (2004) 1198], [astro-ph/0307507]

[34] A. de Oliveira-Costa, M. Tegmark, M. Zaldarriaga and A. Hamilton, *The significance of the largest scale CMB fluctuations in WMAP*, Phys. Rev. **D 69** (2004) 063516, [astro-ph/0307282]

[35] D.J. Schwarz, G.D. Starkman, D. Huterer and C.J. Copi, *Is the low-l microwave background cosmic?*, Phys. Rev. Lett. **93** (2004) 221301, [astro-ph/0403353]

[36] K. Land and J. Magueijo, *The axis of evil*, Phys. Rev. Lett. **95** (2005) 071301, [astro-ph/0502237]

[37] C.J. Copi, D. Huterer, D.J. Schwarz and G.D. Starkman, *On the large-angle anomalies of the microwave sky*, Mon. Not. Roy. Astron. Soc. **367** (2006) 79, [astro-ph/0508047]

[38] H.K. Eriksen, A.J. Banday, K.M. Górski, F.K. Hansen and P.B. Lilje, *Hemispherical power asymmetry in the three-year Wilkinson Microwave Anisotropy Probe sky maps*, Astrophys. J. **660** (2007) L81, [astro-ph/0701089]

[39] J. Hoftuft, H.K. Eriksen, A.J. Banday, K.M. Górski, F.K. Hansen and P.B. Lilje, *Increasing evidence for hemispherical power asymmetry in the five-year WMAP data*, Astrophys. J. **699** (2009) 985, [arXiv:0903.1229]

[40] J. Kim and P. Naselsky, *Anomalous parity asymmetry of the Wilkinson Microwave Anisotropy Probe power spectrum data at low multipoles*, Astrophys. J. **714** (2010) L265, [arXiv:1001.4613]

[41] Y. Akrami, Y. Fantaye, A. Shafieloo, H.K. Eriksen, F.K. Hansen, A.J. Banday and K.M. Górski, *Power asymmetry in WMAP and Planck temperature sky maps as measured by a local variance estimator*, Astrophys. J. **784** (2014) L42, [arXiv:1402.0870]

[42] Planck Collaboration, P.A.R. Ade, N. Aghanim, C. Armitage-Caplan, et al., *Planck 2013 results. XXIII. Isotropy and statistics of the CMB*, Astron. Astrophys. **571** (2014) A23, [arXiv:1303.5083]

[43] Planck Collaboration, P.A.R. Ade, N. Aghanim, Y. Akrami, et al., *Planck 2015 results. XVI. Isotropy and statistics of the CMB*, (2015), arXiv:1506.07135

[44] D.J. Schwarz, C.J. Copi, D. Huterer and G.D. Starkman, *CMB anomalies after Planck*, (2015), arXiv:1510.07929

[45] D.L. Wiltshire, P.R. Smale, T. Mattsson and R. Watkins, *Hubble flow variance and the cosmic rest frame*, *Phys. Rev.* **D 88** (2013) 083529, [arXiv:1201.5371]

[46] J.H. McKay and D.L. Wiltshire, *Defining the frame of minimum nonlinear Hubble expansion variation*, *Mon. Not. Roy. Astron. Soc.* **457** (2016) 3285, [arXiv:1503.04192]

[47] M. Rubart and D.J. Schwarz, *Cosmic radio dipole from NVSS and WENSS*, *Astron. Astrophys.* **555**, A117 (2013), [arXiv:1301.5559]

[48] J.V. Arnau, M.J. Fullana, L. Monreal and D. Sáez, *On the microwave anisotropies produced by a nonlinear voids*, *Astrophys. J.* **402** (1993) 359

[49] J.V. Arnau, M.J. Fullana and D. Sáez, *Great Attractor-like structures and large-scale anisotropy*, *Mon. Not. Roy. Astron. Soc.* **268** (1994) L17

[50] N.P. Humphreys, R. Maartens and D.R. Matravers, *Anisotropic observations in universes with nonlinear inhomogeneity*, *Astrophys. J.* **477** (1997) 47, [astro-ph/9602033].,

[51] K. Tomita, *Bulk flows and cosmic microwave background dipole anisotropy in cosmological void models*, *Astrophys. J.* **529** (2000) 26, [astro-ph/9905278]

[52] H. Alnes and M. Amarzguioui, *CMB anisotropies seen by an off-center observer in a spherically symmetric inhomogeneous universe*, *Phys. Rev.* **D 74** (2006) 103520, [astro-ph/0607334]

[53] K. Bolejko and C. Hellaby, *The Great Attractor and the Shapley Concentration*, *Gen. Rel. Grav.* **40** (2008) 1771, [astro-ph/0604402]

[54] K. Bolejko, C. Clarkson, R. Maartens, D. Bacon, N. Meures and E. Beynon, *Antilensing: The bright side of voids*, *Phys. Rev. Lett.* **110** (2013) 021302, [arXiv:1209.3142]

[55] D.J. Bacon, S. Andrianomena, C. Clarkson, Bolejko, K. and R. Maartens, *Cosmology with Doppler lensing*, *Mon. Not. Roy. Astron. Soc.* **443** (2014) 1900, [arXiv:1401.3694]

[56] K. Bolejko, *The Szekeres Swiss Cheese model and the CMB observations*, *Gen. Rel. Grav.* **41** (2009) 1737, [arXiv:0804.1846]

[57] K. Bolejko and M.N. Célérier, *Szekeres Swiss-cheese model and supernova observations*, *Phys. Rev.* **D 82** (2010) 103510, [arXiv:1005.2584]

[58] A. Nwankwo, M. Ishak and J. Thompson, *Luminosity distance and redshift in the Szekeres inhomogeneous cosmological models*, *JCAP* **05** (2011) 028, [arXiv:1005.2989]

[59] M. Ishak and A. Peel, *The growth of structure in the Szekeres inhomogeneous cosmological models and the matter-dominated era*, *Phys. Rev.* **D 85** (2012) 083502, [arXiv:1104.2590]

[60] K. Bolejko and R.A. Sussman, *Cosmic spherical void via coarse-graining and averaging non-spherical structures*, *Phys. Lett.* **B 697** (2011) 265

[61] R.G. Buckley and E.M. Schlegel, *CMB dipoles and other low-order multipoles in the quasispherical Szekeres model*, *Phys. Rev.* **D 87** (2013) 023524

[62] S.M. Koksbang and S. Hannestad, *Methods for studying the accuracy of light propagation in N-body simulations*, *Phys. Rev.* **D 91** (2015) 043508, [arXiv:1501.01413]

[63] S.M. Koksbang and S. Hannestad, *Studying the precision of ray tracing techniques with Szekeres models*, *Phys. Rev.* **D 92** (2015) 023532; err. ibid. **92** (2015) 069904, [arXiv:1506.09127]

[64] R.A. Sussman, I.D. Gaspar and J.C. Hidalgo, *Coarse-grained description of cosmic structure from Szekeres models*, *JCAP* **03** (2016) 012, [arXiv:1507.02306]

[65] R.A. Sussman and I.D. Gaspar, *Multiple non-spherical structures from the extrema of Szekeres scalars*, *Phys. Rev.* **D 92** (2015) 083533, [arXiv:1508.03127]

[66] B.R. Tully, J.E. Shaya, D.I. Karachentsev, M.H. Courtois, D.D. Kocevski, L. Rizzi and A. Peel, *Our peculiar motion away from the Local Void*, Astrophys. J. **676** (2008) 184, [`arXiv:0705.4139`]

[67] D.L. Wiltshire, *Cosmic clocks, cosmic variance and cosmic averages*, New J. Phys. 9 (2007) 377 [`gr-qc/0702082`]

[68] D.L. Wiltshire, *Exact solution to the averaging problem in cosmology*, Phys. Rev. Lett. **99** (2007) 251101, [`arXiv:0709.0732`]

[69] D.L. Wiltshire, *Average observational quantities in the timescape cosmology*, Phys. Rev. **D 80** (2009) 123512, [`arXiv:0909.0749`]

[70] J.A.G. Duley, M.A. Nazer and D.L. Wiltshire, *Timescape cosmology with radiation fluid*, Class. Quant. Grav. **30** (2013) 175006, [`arXiv:1306.3208`]

[71] M. Kamionkowski and L. Knox, *Aspects of the cosmic microwave background dipole*, Phys. Rev. **D 67** (2003) 063001, [`astro-ph/0210165`]

[72] K. Bolejko, et al., in preparation

[73] N. Li and D.J. Schwarz, *Scale dependence of cosmological backreaction*, Phys. Rev. **D 78** (2008) 083531, [`arXiv:0710.5073`]

[74] M.L. McClure and C.C. Dyer, *Anisotropy in the Hubble constant as observed in the HST extragalactic distance scale Key Project results*, New Astron. **12** (2007) 533, [`astro-ph/0703556`]

[75] H.A. Feldman, R. Watkins and M.J. Hudson, *Cosmic flows on 100 Mpc/h scales: Standardized minimum variance bulk flow, shear and octupole moments*, Mon. Not. Roy. Astron. Soc. **407** (2010) 2328, [`arXiv:0911.5516`]

[76] R.B. Tully, H.M. Courtois, A.E. Dophin, et al., *Cosmicflows-2: The Data*, Astron. J. **146** (2013) 86, [`arXiv:1307.7213`]

[77] P. Erdoğdu, O. Lahav, J.P. Huchra, et al., *Reconstructed density and velocity fields from the 2MASS redshift survey*, Mon. Not. Roy. Astron. Soc. **373** (2006) 45, [`astro-ph/0610005`]

[78] A.G. Riess, L. Macri, S. Casertano, et al., *A 3Space Telescope and Wide Field Camera 3*, Astrophys. J. **730**, 119; (E) **732**, 129, [`arXiv:1103.2976`]

[79] Planck Collaboration, P.A.R. Ade, N. Aghanim, C. Armitage-Caplan, et al., *Planck 2013 results. XVI. Cosmological parameters*, Astron. Astrophys. **571** (2014) A16, [`arXiv:1303.5083`]

[80] E. Hivon, K.M. Górski, C.B. Netterfield, B.P. Crill, S. Prunet and F. Hansen, *Master of the cosmic microwave background anisotropy power spectrum: a fast method for statistical analysis of large and complex cosmic microwave background data sets*, Astrophys. J. **567** (2002) 2, [`astro-ph/0105302`]

[81] G.F.R. Ellis, in *Proceedings of the International School of Physics 'Enrico Fermi' (1971) Course 47: General Relativity and Cosmology*, ed. R.K. Sachs (Academic Press, New York and London), pp. 104–182; reprinted, with historical comments, in *Gen. Rel. Grav.* **41** (2009) 581

[82] R. Sachs, *Gravitational waves in general relativity. VI. The outgoing radiation condition*, Proc. Roy. Soc. Lond. **A 264** (1961) 309

[83] P.J.E. Peebles, *Principles of Physical Cosmology*, (Princeton University Press, 1993)

[84] K. Bolejko and P.G. Ferreira, *Ricci focusing, shearing, and the expansion rate in an almost homogeneous Universe*, JCAP **05** (2012) 003, [`arXiv:1204.0909`]

[85] I.M.H. Etherington, *Phil. Mag.* **15** (1933) 761; reprinted, with historical comments, in *Gen. Rel. Grav.* **39** (2007) 1055

[86] P. Szekeres, *Quasispherical gravitational collapse*, Phys. Rev. **D 12** (1975) 2941

[87] *Planck Legacy Archive* COM_PowerSpect_CMB_R2.01.fits (2013)
http://www.cosmos.esa.int/web/planck/pla

[88] M.F. Struble and H.J. Rood, *A compilation of redshifts and velocity dispersions for ACO clusters*, *Astrophys. J. Suppl.* **125** (1999) 35

[89] H.M. Courtois, D. Pomarède, R.B. Tully, Y. Hoffman, D. Courtois, *Cosmography of the Local Universe*, *Astron. J.* **146** (2013) 69, [arXiv:1306.0091]

[90] Planck Collaboration, N. Aghanim, C. Armitage-Caplan, M. Arnaud, et al., *Planck 2013 results. XXVII. Doppler boosting of the CMB: Eppur si muove*, *Astron. Astrophys.* **571** (2014) A27, [arXiv:1303.5087]

[91] M.J. Rees and D.W. Sciama, *Large-scale density inhomogeneities in the universe*, *Nature* **217** (1968) 511

[92] A. Rakic, S. Räsänen and D.J. Schwarz, *Microwave sky and the local Rees-Sciama effect*, *Mon. Not. Roy. Astron. Soc.* **369** (2006) L27, [arXiv:, [astro-ph/0601445]

[93] K.T. Inoue and J. Silk, *Local voids as the origin of large-angle cosmic microwave background anomalies*, *Astrophys. J.* **648** (2006) 23, [astro-ph/0602478]

[94] A. Meszaros and Z. Molnar, *On the alternative origin of the dipole anisotropy of microwave background due to the Rees-Sciama effect*, *Astrophys. J.* **470** (1996) 49